



## RESEARCH ARTICLE

10.1029/2021MS002658

**Key Points:**

- Upper ocean processes relevant to MJO simulations in the Climate Forecast System are improved through our Climate Process Team project
- Realistic model simulations of diurnal warming and its dependence on mixing schemes are demonstrated by the comparison with in situ data
- A series of CFS simulations indicate a positive impact of high vertical resolution near the ocean surface on MJO prediction skills

**Correspondence to:**

T. Shinoda,  
toshiaki.shinoda@tamu.edu

**Citation:**

Shinoda, T., Pei, S., Wang, W., Fu, J. X., Lien, R.-C., Seo, H., & Soloviev, A. (2021). Climate Process Team: Improvement of ocean component of NOAA Climate Forecast System relevant to Madden-Julian Oscillation simulations. *Journal of Advances in Modeling Earth Systems*, 13, e2021MS002658. <https://doi.org/10.1029/2021MS002658>

Received 15 JUN 2021  
Accepted 28 SEP 2021

© 2021 The Authors. Journal of Advances in Modeling Earth Systems published by Wiley Periodicals LLC on behalf of American Geophysical Union. This is an open access article under the terms of the Creative Commons Attribution-NonCommercial License, which permits use, distribution and reproduction in any medium, provided the original work is properly cited and is not used for commercial purposes.

## Climate Process Team: Improvement of Ocean Component of NOAA Climate Forecast System Relevant to Madden-Julian Oscillation Simulations

Toshiaki Shinoda<sup>1</sup> , Suyang Pei<sup>1</sup> , Wanqiu Wang<sup>2</sup> , Joshua X. Fu<sup>3</sup> , Ren-Chieh Lien<sup>4</sup> , Hyodae Seo<sup>5</sup> , and Alexander Soloviev<sup>6</sup>

<sup>1</sup>Texas A&M University - Corpus Christi, Corpus Christi, TX, USA, <sup>2</sup>NOAA/NCEP/CPC, Camp Springs, MD, USA, <sup>3</sup>University of Hawaii, Honolulu, HI, USA, <sup>4</sup>APL/University of Washington, Seattle, WA, USA, <sup>5</sup>Woods Hole Oceanographic Institution, Falmouth, MA, USA, <sup>6</sup>Nova Southeastern University, Fort Lauderdale-Davie, FL, USA

**Abstract** Given the increasing attention in forecasting weather and climate on the subseasonal time scale in recent years, National Oceanic and Atmospheric Administration (NOAA) announced to support Climate Process Teams (CPTs) which aim to improve the Madden-Julian Oscillation (MJO) prediction by NOAA's global forecasting models. Our team supported by this CPT program focuses primarily on the improvement of upper ocean mixing parameterization and air-sea fluxes in the NOAA Climate Forecast System (CFS). Major improvement includes the increase of the vertical resolution in the upper ocean and the implementation of General Ocean Turbulence Model (GOTM) in CFS. In addition to existing mixing schemes in GOTM, a newly developed scheme based on observations in the tropical ocean, with further modifications, has been included. A better performance of ocean component is demonstrated through one-dimensional ocean model and ocean general circulation model simulations validated by the comparison with in-situ observations. These include a large sea surface temperature (SST) diurnal cycle during the MJO suppressed phase, intraseasonal SST variations associated with the MJO, ocean response to atmospheric cold pools, and deep cycle turbulence. Impact of the high-vertical resolution of ocean component on CFS simulation of MJO-associated ocean temperature variations is evident. Also, the magnitude of SST changes caused by high-resolution ocean component is sufficient to influence the skill of MJO prediction by CFS.

**Plain Language Summary** The idea of Climate Process Teams (CPTs) has been suggested in early 2000 to accelerate the development of numerical models for prediction of weather and climate. Members of CPTs consist of observationalists, theoreticians, process-oriented modelers, and scientists at modeling centers, and thus knowledge obtained from observational and process-oriented researches can be transferred to the improvement of physical process representations in global climate models. The CPT program initiated by NOAA in 2015 specifically aims to improve prediction of Madden-Julian Oscillation (MJO) which is the major intraseasonal (30–90 days) fluctuation in the tropical atmosphere. Our CPT primarily focuses on improving the representation of upper ocean processes relevant to the MJO in NOAA's operational climate prediction system: Climate Forecast System (CFS). Performance of the improved ocean component of CFS is evaluated through a comparison of model simulations with high-quality in-situ data collected during the recent field campaign which was designed to monitor ocean and atmospheric variability associated with the MJO. The improvement includes the realistic model simulation of large upper ocean warming during daytime through implementing high vertical resolution mixing schemes near the surface. The results demonstrate a significant impact of the high-vertical resolution ocean component in CFS on the MJO prediction skill.

### 1. Introduction

The concept of “Climate Process Team (CPT)” has been developed by US CLIVAR in early 2000 to improve large-scale IPCC-class coupled climate models (US CLIVAR Scientific Steering Committee, 2002). The aim of the CPT concept is to accelerate the development of global coupled climate models and reduce errors in climate models by bringing together field observationalists, theoreticians, process-oriented modelers, and scientists at modeling centers to concentrate on improving the realism in the simulation of processes in

the climate system. Hence, the model improvement by CPTs is achieved through facilitating the transfer of knowledge from observational and process-oriented research to the development of physical process representations (parameterizations) in ocean or atmospheric component of global climate models (<https://usclivar.org/climate-process-teams>). Over the past decades, several CPTs have been formed and contributed to model improvement substantially on many aspects in climate models (e.g., Bretherton et al., 2004; Legg et al., 2009; MacKinnon et al., 2017; Subramanian et al., 2016).

In 2015, National Oceanic and Atmospheric Administration (NOAA) Climate Variability and Predictability (CVP) program has announced to support CPTs that focus on specific areas of atmospheric and oceanic processes. Unlike other past CPT programs supported by government agencies, this NOAA CPT announcement focuses on fairly specific aspects of climate models, which support “CPT that will use the data collected during the international field campaign, Dynamics of the Madden Julian Oscillation (DYNAMO), and other observations, to identify and improve processes that affect MJO initiation and propagation in the NOAA weather and climate models.” (referred to as “NOAA DYNAMO CPT” hereafter). Such narrowly defined topic with relatively smaller size of the team is consistent with the recommendations made by US CLIVAR in 2008 (U.S. CLIVAR Office, 2008).

DYNAMO field campaign is the US component of CINDY2011 (Cooperative Indian Ocean Experiment on Intraseasonal Variability in Year 2011), an international field program during September 2011–March 2012 in the tropical central Indian Ocean. A major goal of DYNAMO is to expedite our understanding of the physical and dynamical processes key to Madden-Julian Oscillation (Madden & Julian, 1972) initiation in the Indian Ocean and improving our ability to simulate and forecast the MJO (Yoneyama et al., 2013; Zhang et al., 2013). During the field campaign, three active episodes of large-scale convection associated with the MJO propagated eastward across the tropical Indian Ocean (e.g., Gottschalck et al., 2013; Shinoda et al., 2013). Accordingly, upper-ocean and atmospheric variability associated with these MJO events were well monitored in the DYNAMO areas as a substantial amount of high quality in-situ data of the atmosphere and ocean in the central tropical Indian Ocean have been collected.

Our team supported by NOAA DYNAMO CPT specifically focuses on upper ocean processes relevant to the MJO simulations in the NOAA Climate Forecast System (CFS; Saha et al., 2014). There is growing evidence that air-sea coupled processes largely influence MJO simulations (e.g., DeMott et al., 2015; Flatau et al., 1997; Fu et al., 2017; Seo et al., 2014; Shinoda et al., 1998; Zhang et al., 2006). The upper ocean processes and equatorial wave dynamics influence the mixed-layer heat content, stratification, and mixing, thereby sea surface temperature (SST; e.g., Shinoda & Hendon, 2001; Zhang & Anderson, 2003); ensuing anomalous air-sea flux modulates the deep convection, surface winds and shortwave radiation, which in turn generate intraseasonal variation in SST. Hence oceanic processes are of great importance to MJO initiation, development, and propagation, because they are fundamental in determining SST and atmospheric convection is very sensitive to small changes in SSTs especially in the tropical Indian Ocean where SST is higher than 28°C in most regions. Accordingly, adequate representations of upper ocean processes in the ocean component of coupled climate models could largely influence MJO simulations.

A major objective of our CPT project is to improve representations (parameterizations) of upper ocean mixing processes that directly influence SSTs on the intraseasonal time scale in CFS. In addition, algorithm of surface flux computation has been updated with the most recent version. Skills of SST simulations associated with MJO events by ocean component of CFS have been evaluated based on the comparison with in-situ and satellite observations, including the DYNAMO data. The impact of the improved representations of upper ocean processes on MJO simulations in CFS has been further evaluated.

In this paper, major model improvement resulting from our CPT project is summarized. To evaluate mixing parameterizations, various model experiments using one-dimensional (1-D) ocean models and an ocean general circulation model (ocean component of CFS) were conducted, and thus results from these ocean model experiments integrated by given surface forcing fields are primarily described. The impact of ocean mixing parameterization on MJO simulations during DYNAMO is also discussed based on a series of CFS simulations.

## 2. Improvement of CFS Ocean Component

As discussed in the introduction section, upper ocean processes may largely impact MJO simulations. In particular, previous studies suggest that large diurnal warming during the suppressed phase of the MJO plays an important role in air-sea interaction processes associated with the MJO (e.g., Bellenger et al., 2010; Bernie et al., 2007; Li et al., 2013; Seo et al., 2014; Shinoda & Hendon, 1998; Shinoda, 2005; Woolnough et al., 2001). Since the diurnal warming in the Indo-Pacific warm pool region occurs mostly in the upper few meters, a high vertical resolution in the upper 10-m is crucial to adequately represent such warming during daytime in models (e.g., Bernie et al., 2005). Also, heat advection and ocean mixing (entrainment) generated by strong eastward currents in the near surface layer associated with westerly winds could influence MJO propagation (e.g., Flatau et al., 1997). For example, vertical shear associated with wind-driven currents enhances entrainment cooling and in turn affects the atmospheric variability, and thus vertical shear needs to be realistically simulated by the ocean component. Also, the evolution of upper ocean currents largely depends on the momentum flux near the surface which is determined by vertical profile of current shear. Both the diurnal warming and near-surface vertical shear could largely depend on mixing schemes used in the upper layer. Hence, the major changes of the ocean component of CFS in this study include the increase of vertical resolution near the ocean surface and the implementation of General Ocean Turbulence Model (GOTM; Burchard et al., 1999; Umlauf et al., 2005) in which several different mixing schemes are available. The details of these changes are described in this section.

The ocean component of the current version of operational CFS is the GFDL Modular Ocean Model version 4 (MOM4). The vertical mixing in MOM4 used in CFS is the K profile parameterization (KPP: Large et al., 1994), where the vertical resolution of ocean component near the surface is about 10 m. Because of the structure of model code in MOM4, it requires substantial changes to increase the vertical resolution near the surface. Hence MOM4 has been first replaced with the Modular Ocean Model version 5 (MOM5) to allow the modification of the vertical resolution.

As discussed above, the vertical resolution needs to be improved especially for the simulation of tropical variability on diurnal to intraseasonal time scales. Large diurnal warming in the upper few meters could play an important role in air-sea interaction processes associated with the MJO. As demonstrated in previous one-dimensional ocean model simulations (e.g., Bernie et al., 2005; Shinoda, 2005), 1-m vertical grid spacing is sufficient for simulating observed large diurnal warming in the Indian and western Pacific warm pool. Therefore, the vertical resolution has been changed to 1-m in the upper 10-m where the diurnal warming primarily occurs.

The KPP vertical mixing scheme is shown to perform reasonably well especially for the relatively low vertical resolutions. However, for the model with a fine resolution near the surface, it is still uncertain whether other mixing schemes could be more suitable. Also, the performance of different mixing schemes may depend on atmospheric conditions. Given that many other vertical mixing schemes have been developed in the past and different performance of some of the schemes have been demonstrated in certain atmospheric conditions (e.g., Pei et al., 2018), it is at least beneficial to include multiple vertical mixing schemes in coupled prediction systems.

In this study, General Ocean Turbulence Model (GOTM), which includes several different vertical mixing schemes, has been implemented in the ocean component of CFS, and the vertical resolution has been increased to 1-m. GOTM is designed to be easily coupled to 3-D circulation models, and to be used as a module for the computation of vertical turbulent mixing. Although not all turbulence models published in oceanography are implemented, at least one member of every relevant model family can be found in GOTM, including KPP (Large et al., 1994), Mellor and Yamada (1982), and Canuto et al. (2001).

In addition to existing schemes in GOTM, another scheme developed based on in situ measurements in the western Pacific warm pool (Soloviev et al., 2001; referred to as “SLH scheme” hereafter) has been modified for GOTM framework and included. In the SLH scheme, mixing coefficients within the mixed layer are parameterized as a function of gradient Richardson number ( $Ri$ ) and friction velocity  $u^*$ . The scheme performs well in the western equatorial Pacific where turbulent boundary layers are highly non-stationary and heterogeneous (e.g., Huyer et al., 1997; Soloviev & Lukas, 1997). Given the reasonable performance of SLH scheme under different atmospheric conditions over the warm pool region (Soloviev et al., 2001) where

the MJO convection is developed and propagated, the inclusion of this scheme may significantly impact the MJO simulations in coupled prediction systems. It should be noted that reasonable performance of SLH scheme has also been demonstrated in other areas (Katsaros & Soloviev, 2004; Katsaros et al., 2005; Soloviev et al., 2002).

The SLH scheme originally described in Soloviev et al. (2001) has been further modified for implementation to MOM5. One of the major problems of original SLH scheme was the very large mixing coefficient produced under a very unstable regime of the model. In the original version of SLH scheme, the mixing coefficient  $K_x$  is calculated by

$$K_x = \kappa u^* z (a_x - c_x R_i)^{1/3} \quad R_i < R_{ix}$$

where  $\kappa = 0.4$  is von Karman's constant,  $a_x$  and  $c_x$  are constants determined by observations, and the subscript  $x$  is  $m$  or  $s$ , representing momentum or scalar. For instance,  $R_{im} = -0.2$  and  $R_{is} = -1.0$  define the Richardson number of a very unstable regime for momentum and scalar mixing. Within the very unstable regime, such as a state close to pure convection, the negative Brunt-Väisälä frequency and the vanishing vertical shear could make  $R_{ix}$  a very large negative number, and thus producing unrealistic large mixing coefficients. In the modified version,  $K_x$  is calculated by

$$K_x = \kappa z (a_x u^{*3} + c_x \kappa \sigma w^{*3})^{1/3} \quad Ri < R_{ix}$$

in which  $w^*$  is the convective velocity scale and  $\sigma$  is a dimensionless vertical coordinate (see Large et al., 1994). Note as  $u^* \rightarrow 0$ ,  $K_x \propto w^*$  is the correct scaling for convection. To avoid the unrealistic large mixing coefficients,  $\sigma$  is constrained to a maximum value of 0.1,

$$\sigma = \min(z/h, 0.1)$$

This constraint is same as that used in the KPP scheme. Also, the critical Richardson number of the model  $Ri_{cr}$  that determines the mixed layer depth has been changed to 0.4 from 0.25 based on the recent experiments and large-eddy simulations (Canuto et al., 2001; Cheng et al., 2002; Large et al., 1994; Peters et al., 1988; Wang et al., 1996; Zaron & Moum, 2009).

In this study, five vertical mixing parameterizations, which are referred to as K-profile parameterization (KPP), SLH,  $k$ - $\epsilon$ , Generic Length (GL), and Mellor and Yamada (MY) schemes, are evaluated based on the comparison with observations in the following sections. KPP (Large et al., 1994) is a first order empirical turbulent closure model in which non-local transport of vigorous convection is included. GL,  $k$ - $\epsilon$ , and MY schemes are second moment closure turbulence models. These schemes all solve dynamic equations of turbulence kinetic energy but differ on how the turbulence length scale is computed and how the stability functions are determined. The GL scheme uses dynamic  $k$  and generic length scale equations for the closure (Umlauf & Burchard, 2003) where  $k$  represents the turbulent kinetic energy, and the stability function is following Canuto et al. (2001). The  $k$ - $\epsilon$  scheme (Rodi, 1987; Burchard & Bolding, 2001) uses dynamic  $k$  and  $\epsilon$  equations for the closure where  $\epsilon$  represents the rate of dissipation of turbulent kinetic energy, with its stability function same as the GL scheme. The MY scheme (Mellor & Yamada, 1982) uses  $q^2$  and  $q^2 l$  equations for the closure where  $q$  and  $l$  represent a velocity scale and length scale, respectively, and the stability function is computed based on Cheng et al. (2002). Further details of these schemes are described in the references cited above.

In addition to the implementation of vertical mixing parameterization, air-sea flux algorithm used to calculate surface heat fluxes (Long 1984, 1986; Zeng et al., 1998) are replaced by COARE bulk flux algorithm version 3.5 (COARE3.5; Edson et al., 2013; Fairall et al., 2003). The impact of the use of COARE3.5 on latent heat flux and SST is evaluated by OGCM simulations.

In the following section, the evaluation of the GOTM including the SLH scheme using 1-D model simulations is first provided based on the comparison with the DYNAMO data. Then the improved MOM5 with GOTM is evaluated by comparing with the observations. Finally, the evaluation of MJO simulation by CFS

with the improved ocean component is discussed based on a set of forecast experiments for the MJO event observed during DYNAMO.

### 3. Model Evaluations

Since the primary focus in this study is the improvement of ocean processes relevant to MJO simulations, the model evaluations focus on diurnal to intraseasonal SST variability, and associated temperature and velocity variations in the upper ocean. In particular, as briefly discussed in previous section, a diurnal variation of SST during the suppressed phase may impact initiation of MJO convection in the active phase (e.g., Seo et al., 2014). The simulated diurnal variations are compared with in situ data. While previous studies on model validations of wind-generated ocean currents mostly focus on the comparison of upper ocean velocity (e.g., Shinoda et al., 2016, 2017), the vertical shear is more relevant to the vertical mixing parameterizations and evolution of vertical shear in turn affect the vertical profile of wind-driven currents. Yet, there are few quantitative comparisons of vertical shear between the model and observations because of the lack of high-resolution in situ velocity measurements in key locations.

During DYNAMO, comprehensive data of upper ocean variability which can adequately resolve diurnal warming and vertical shear (Chi et al., 2014; Yoneyama et al., 2013) have been collected and processed. These include hydrographic and velocity data measured by surface and subsurface moorings in the central Indian Ocean (Chi et al., 2014, 2021). The data from these moorings are primarily used for model validations in this study.

Vertical mixing schemes implemented in MOM5 are first evaluated in one-dimensional ocean model simulations at the DYNAMO mooring locations. Since the DYNAMO data include surface forcing fields, the 1-D model can be integrated with accurate surface forcing and thus the error in the ocean variability caused by surface fluxes can be minimized. Then OGCM simulations using modified MOM5 are conducted to evaluate the model's ability to simulate diurnal and intraseasonal upper ocean variations based on the comparison with the observational data. Finally, MJO simulations by CFS with improved ocean components are evaluated.

#### 3.1. One-Dimensional Ocean Model Simulations

1-D models are integrated with accurate surface fluxes estimated from DYNAMO observations. Two surface moorings were deployed at  $0^{\circ}$ ,  $79^{\circ}\text{E}$  and  $1.5^{\circ}\text{S}$ ,  $79^{\circ}\text{E}$  in mid-September 2011 and recovered in late January 2012. The meteorological sensors in the mooring at  $0^{\circ}$ ,  $79^{\circ}\text{E}$  were vandalized on 20 November 2011. Hence the 1-D model simulations are conducted for the entire period of the mooring observations at  $1.5^{\circ}\text{S}$ ,  $79^{\circ}\text{E}$  while the integrations for the  $0^{\circ}$ ,  $79^{\circ}\text{E}$  location are conducted up to 20 November. Since the period for simulations at  $1.5^{\circ}\text{S}$ ,  $79^{\circ}\text{E}$  covers all three MJO events during DYNAMO, the comparison of the model results at this location is primarily shown.

Previous studies indicate that diurnal and intraseasonal variations of SST associated with the MJO are sensitive to the formulation of penetrative component of solar radiation in models (e.g., Shinoda & Hendon, 1998; Shinoda, 2005). During DYNAMO, optical profiles in the upper ocean are measured by R/V *Revelle* in 5–27 October and 11 November–2 December at the location close to the mooring observation ( $0^{\circ}$ ,  $80.5^{\circ}\text{E}$ ; Moum et al., 2014). 1-D models were integrated using the in situ optical profile for these periods. Since in situ optical profile is shown to be very close to the double exponential function of Jerlov water type 1A (Paulson & Simpson, 1977), models were also integrated using the penetrative solar radiation profile with  $e$ -folding length scales of the water type 1A for the entire period of DYNAMO. No significant difference is found between these two methods (Pei et al., 2018). The model results using the water type 1A profile are mostly shown in this section, but the diurnal variations simulated by those with the in situ optical profile are shown in Section 3.1.2.

##### 3.1.1. Intraseasonal SST Variation

Figure 1 shows the time series of SST from observations at  $1.5^{\circ}\text{S}$ ,  $79^{\circ}\text{E}$  and 1-D models with different mixing schemes (KPP, SLH, GL,  $k\text{-}\epsilon$ , MY). The vertical resolution of 1-D models is 0.5-m and thus the first grid represents the temperature at 0–0.5 m depth. Since the shallowest temperature sensor of the mooring is

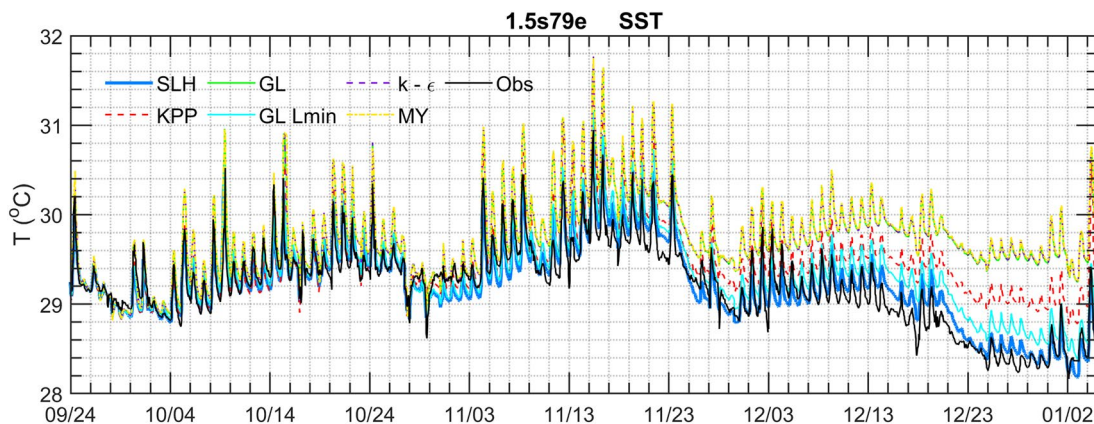


**Figure 1.** Time series of SST at  $1.5^{\circ}\text{S}$ ,  $79^{\circ}\text{E}$  during DYNAMO from simulations of SLH (blue line),  $k-\epsilon$  (purple dashed line), Mellor and Yamada (yellow dash-dotted line), KPP (red dashed line), GL (solid green line), GL with minimum mixing length of 0.5 m (solid light blue line), and observations (black line).

located at  $0.75\text{ m}$  ( $1.5^{\circ}\text{S}$ ,  $79^{\circ}\text{E}$ ) and  $0.66\text{ m}$  ( $0^{\circ}$ ,  $79^{\circ}\text{E}$ ), the sea surface temperature (SST), which is linearly interpolated to the sensor depth using nearest two grid points in models, is used for the comparison.

Overall, observed intraseasonal variations and the associated diurnal variation change are well captured by all models. In particular, the SST warming during suppressed phase of first two MJOs (mid-October and mid-November) and the cooling during the active phase (late October and late November) are well simulated by all models.

However, during the suppressed phase in mid-November after the MJO convection passed over the mooring locations, some of the models ( $k-\epsilon$ , GL, MY) start generating SSTs warmer than observations. These warm biases continue to grow, and near the end of third MJO event in late December to early January, SSTs in these models are warmer by about  $1^{\circ}\text{C}$ . The warm bias is minimum in the SLH scheme in the end of December in which errors are within  $0.2^{\circ}\text{C}$ . It is found that such biases could be reduced by changing the value of model parameters in some models. For example, we have conducted the same simulation using the GL scheme by imposing a minimum mixing length of  $0.5\text{ m}$  (see the next section for the detail), and the warm bias is largely reduced (light blue line in Figure 1). Since these are the results of 1-D models, discrepancies between models and observations could be caused by a combination of model deficiencies and 3-D oceanic processes which are not included in models. Therefore, it is not possible to rank these schemes by this comparison only. Nevertheless, the results show that all schemes perform reasonably well in simulating intraseasonal SST variations, and the gradual drift of SST in some models are within the possible bias caused by 3-D processes. In addition, the model performance could be further improved by changing some of the model parameters.

### 3.1.2. Diurnal Cycle of SST

Diurnal variations of SST simulated by 1-D models and observed by DYNAMO moorings are shown in Figure 2. Figure 2a shows a large amplitude of diurnal SST warming ( $0.8\text{--}1^{\circ}\text{C}$ ) events observed at  $0^{\circ}$ ,  $79^{\circ}\text{E}$  on 14–16 November. While all models generate the SST diurnal warming which is comparable to that from observations, there are significant differences. The amplitude of warming in the SLH model is close to observations, but second moment turbulence closure models (MY, GL,  $k-\epsilon$ ) overestimate the SST warming by about 50%. The SST amplitude simulated by the KPP model is between the SLH and second moment turbulence closure models.

To further examine general characteristics of model performance, the composite diurnal SST variations are constructed from models and observations (Figure 2b). The composites are calculated by averaging the SST time series of all dates in which the amplitude of SST diurnal variation exceeds one standard deviation. The amplitude is defined by the daily maximum SST minus daily minimum SST divided by 2 (e.g., Shinoda, 2005). The composite was formed by averaging the data of 9 dates selected by the criteria above.

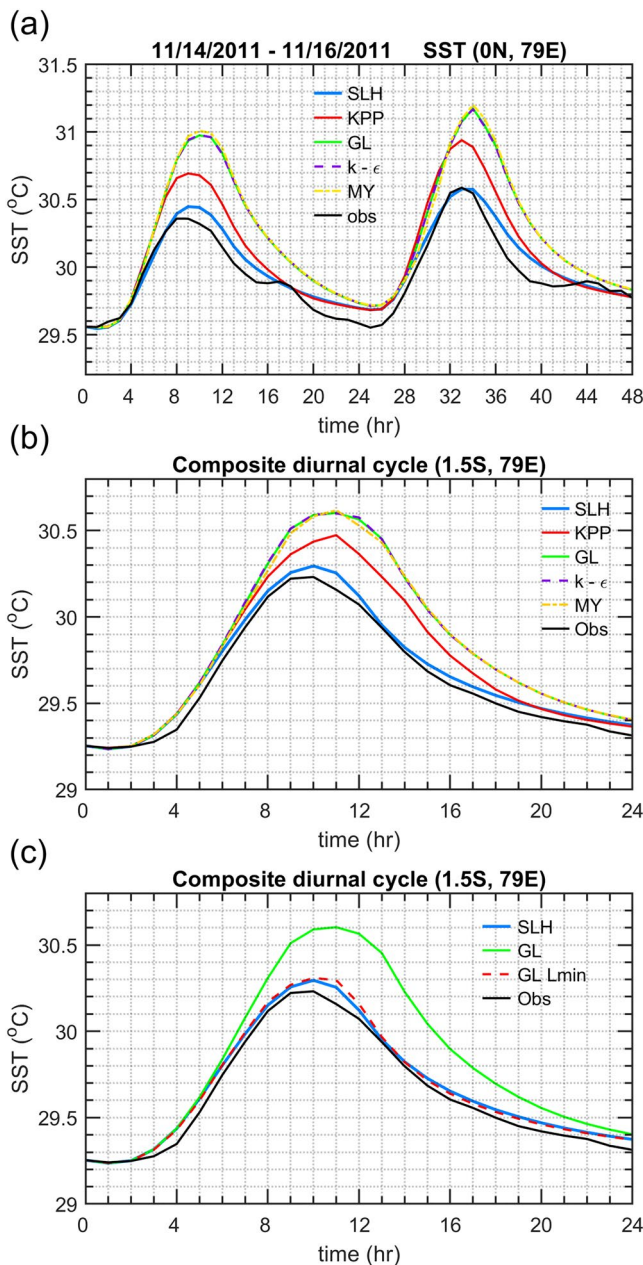


**Figure 2.** (a) The time series of SST at  $0^{\circ}$ ,  $79^{\circ}\text{E}$  for the period of strong diurnal cycle during DYNAMO from the simulations using different vertical mixing schemes and observations. Time 0 in the horizontal axis represents 5:00 LST. The colors of lines indicate the mixing scheme, which are the same as Figure 1. (b) Same as (a) except for the composite diurnal SST at  $1.5^{\circ}\text{S}$ ,  $79^{\circ}\text{E}$ . (c) Same as (b) except that only SLH, GL, GL with minimum mixing length of 0.5 m, and observation are shown.

The difference between models in the composite of entire DYNAMO period is shown to be similar to the case study (Figure 2a) in which the second moment turbulence closure models overestimate the amplitude (Figure 2b). One possible reason for the overestimation of SST diurnal amplitude could be too weak mixing below the shallow mixed layer under the condition of very stable stratification. The weak mixing under stable conditions is often provided by constant background mixing in OGCMs which represents processes that are not properly modeled (e.g., internal waves, double diffusion).

While the default version of 1-D models in GOTM does not include such background mixing, it can be included by changing the model parameter. For example, in GL model, a lower limit of turbulence length scale can be imposed to provide additional background mixing. Figure 2c shows the diurnal SST simulated by the GL scheme in which a lower limit of the turbulence length scale is specified as 0.5 m, and it is compared with the one simulated by the original version of GL model with no minimum length scale limit. The magnitude of diurnal warming in the simulation is significantly reduced and closer to observations by specifying the turbulence mixing length scale limit. This suggests that mixing below the mixed layer due to interior shear and internal gravity waves is underestimated in the GL model and that such mixing is at least partly accounted for SLH scheme with the  $Ri$ -dependent parameterization. As discussed in the previous section, the warm bias of SST during the third MJO event (mid-December–Early January) is also reduced significantly by specifying the minimum mixing length scale (Figure 1).

### 3.1.3. Vertical Velocity Shear

Because of ocean dynamical processes, it is generally difficult to use observed velocity fields to validate mixing parameterization in 1-D modeling framework. For example, the acceleration of zonal velocity near the equator generated by zonal winds could be reduced after a pressure gradient force is formed by sea surface height (SSH) changes associated with divergence/convergence of zonal currents, but such horizontal pressure gradient is not generated in 1-D models. Therefore, large discrepancies in near-surface velocity between 1-D models and observations are often found especially near the equator. However, it is found that vertical shear of horizontal velocity (instead of velocity) is a suitable variable to evaluate the mixing scheme since the evolution of shear is primarily determined by the vertical mixing. The time series of vertical shear defined as the difference in meridional velocity between 6- and 20-m depths from 1-D models and observations are shown in Figure 3. Although the integration period is relatively long (more than 3 months), the velocity shear in 1-D models agrees reasonably well with observations for the entire period. Note that a similar agreement between observations and model simulations is found in the vertical shear of zonal velocity (not shown). Note also that the velocity of 1-D models deviates substantially from observations during this period (not shown).

To examine the sensitivity of model's shear with the vertical resolution, models with 1- and 10-m vertical resolutions are integrated (Figures 3a and 3b). Overall, both 1- and 10-m resolution models perform reasonably well. However, larger differences between models and observations are found in the 10-m resolution run, suggesting that the use of fine vertical resolution is crucial for the accurate simulation of vertical shear. While previous studies indicate that the use of fine vertical resolution largely improves the diurnal SST

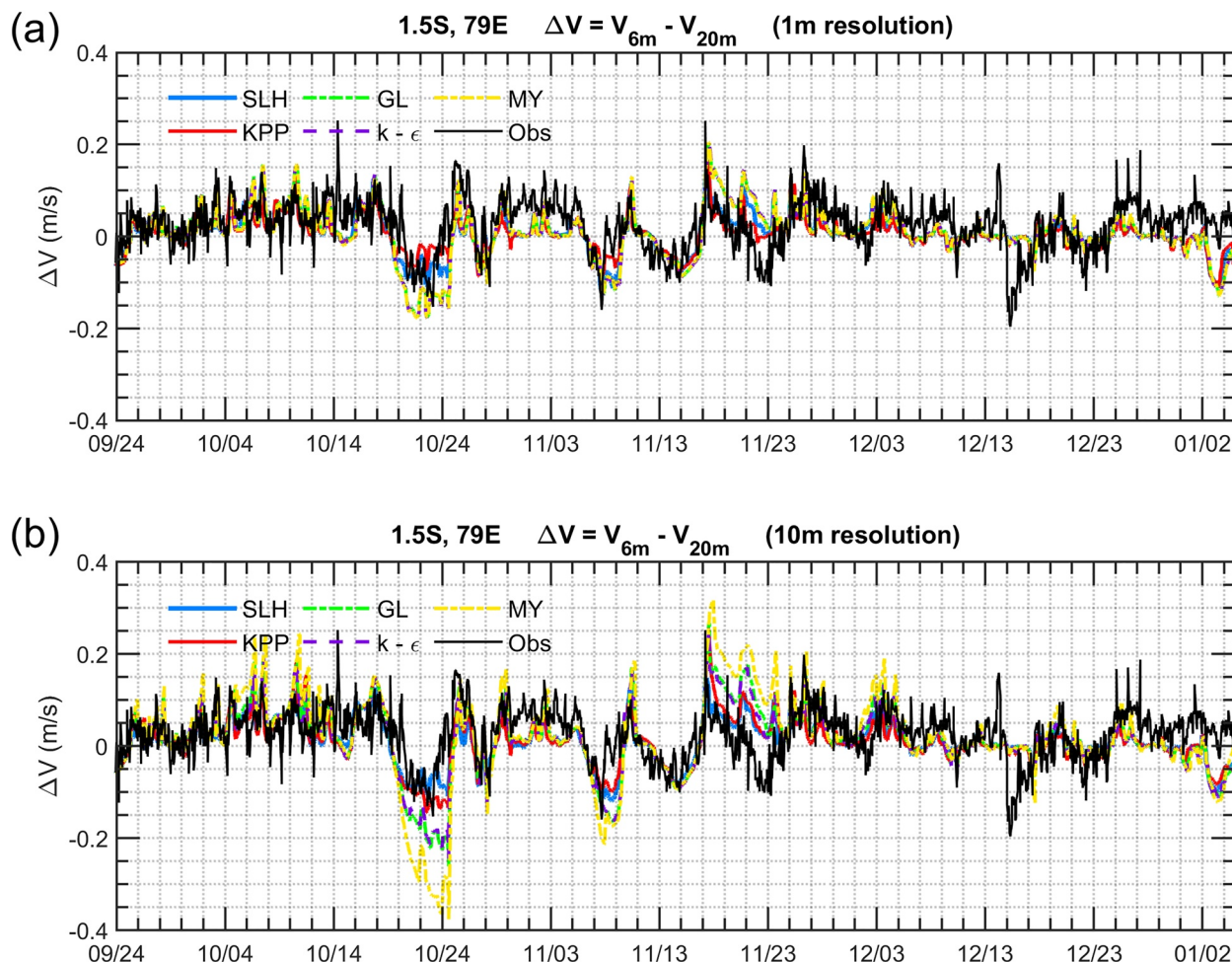


**Figure 3.** (a) Time series of difference in meridional velocity between 6-m and 20-m depths from 1-D model simulations with 1-m vertical resolution, SLH (blue), KPP (red), GL (green), MY (yellow),  $k-\epsilon$  (purple), and observations (black). (b) Same as upper panel except for 10-m vertical resolution.

simulations (e.g., Ge et al., 2017), the result suggests that the velocity structure near the surface in models could also be improved by the use of a finer vertical resolution.

The large discrepancies are found during specific periods such as 18–24 October and 17–23 November. The sign of the shear changes during these periods. During 18–24 October, the currents at 20 m are reduced as currents at 6 m become weak in SLH model, while the 20 m current reduction in second moment turbulence closure models (MY, GL,  $k-\epsilon$ ) delays, and the delay of the velocity reduction at this depth is more prominent for 10-m resolution models (not shown). During this period, a rapid change of zonal wind direction occurs on 17 October (Figure 4) while the large diurnal warming is maintained (Figure 1). As discussed in the previous section, the mixing below the mixed layer during the period of strong diurnal cycle in the second moment closure models is too weak and thus the momentum flux change at the surface may not penetrate enough to change the direction of the current at 20 m. Similar changes of winds for 1–2 days are also found on 16 and 17 November. A large diurnal warming is also maintained in this period until MJO convection onset occurs in late November. Since these periods of relatively large changes of vertical shear occurs during the MJO suppressed phase, stable stratification is maintained and the large SST diurnal cycle is observed. Hence these results are consistent with those in the previous section in which mixing below the mixed layer during stable conditions is too weak in second moment turbulence closure models.

To further investigate the realism of vertical shear in models, the vertical structure of simulated shear is compared with that estimated from in situ measurements. In observations, the strongest shear is frequently found around 60 m depth and a similar magnitude of shear is also found occasionally in the shallower layer

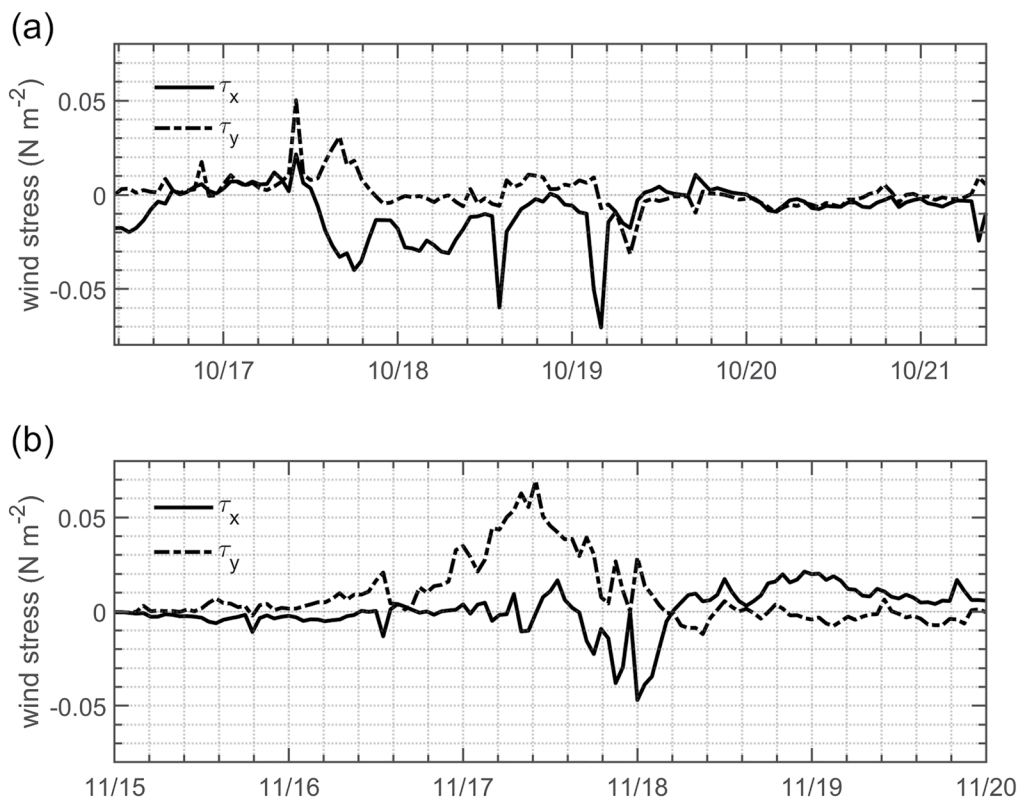


**Figure 4.** (a) Zonal (solid line) and meridional (dashed-dotted line) wind stress at 1.5°S, 79°E estimated from the mooring observations for the period 16–21 October 2011. (b) Same as (a) except for the period 15–19 November.

around 30 m. Such structures are simulated by the SLH scheme (Figure 5), suggesting that  $Ri$ -dependent mixing scheme can reproduce a realistic structure of vertical shear. In the simulation by KPP, the strong shear is largely concentrated around 50–60 m depths which is much stronger than observations and such strong shear are rarely found in shallower areas. A similar structure of strong shear which is concentrated around 60 m depth is also found in the  $k$ - $\epsilon$  model.

### 3.1.4. Ocean Response to Atmospheric Cold Pools

Atmospheric cold pools are pools of cold air which are formed as convective downdrafts caused by evaporation of rainwater that originates from above the atmospheric boundary layer (e.g., Zipser, 1977; Zuidema et al., 2017). During DYNAMO, cold pools were frequently observed (e.g., Chen et al., 2016; de Szoeke & Edison, 2017; Feng et al., 2015; Yokoi et al., 2014). Figures 6a and 6b show the surface freshwater flux and wind stress associated with the strong cold pool event observed at 1.5°S, 79°E on 27–28 October 2011, respectively. Intense precipitation is found during 3–14 h with an average rain rate of 14.7 mm/h (Figure 6a), followed by strong westerly winds which generate more than 0.4  $\text{N/m}^2$  of wind stress (Figure 6b). Such heavy rain and strong winds cause large ocean response including rapid drop of temperature in the very shallow mixed layer (Figure 6c).

Upper ocean variability produced by such unique atmospheric events provides an excellent case for testing vertical mixing schemes (Pei et al., 2018). During the cold pool event, SST dropped to their minimum value within 15 h from the beginning of the event by large evaporative cooling, yet the depth of mixed layer is only 0.75 m at the time of minimum SST as a result of heavy precipitation. Then the SST gradually recovers despite the surface heat flux is still negative (cooling the ocean, not shown). Some of the 1-D models in GOTM is integrated for this cold pool event using surface forcing fields observed by the DYNAMO mooring. PWP model (Price et al., 1986) is also used for the comparison in this case. SST variations induced by cold pool are simulated reasonably well by all models (Figure 6d). However, SLH, KPP and PWP models perform significantly better than second moment turbulent closure models (GL,  $k$ - $\epsilon$ , MY) which generate SSTs colder than

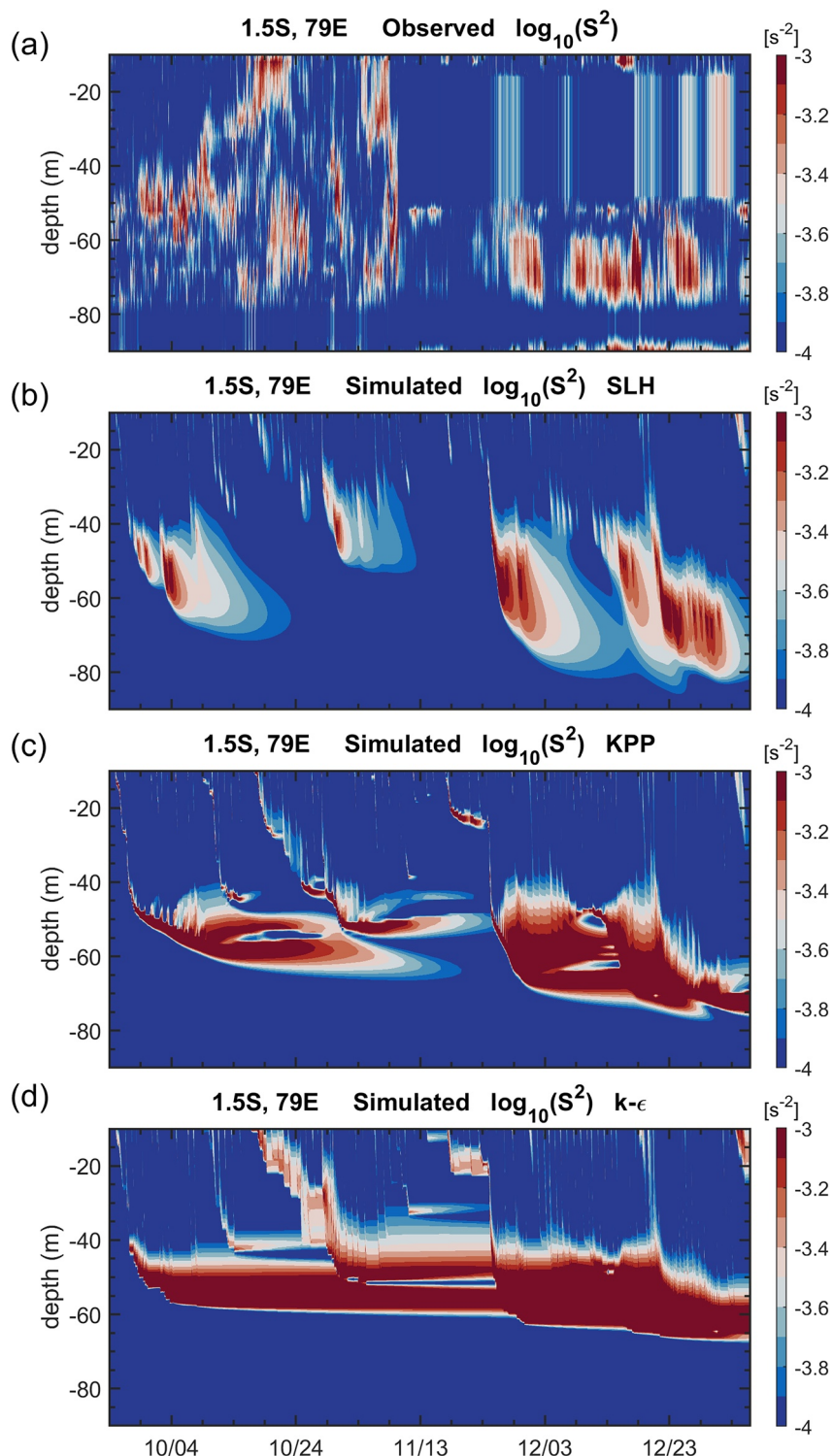


**Figure 5.** Time series of vertical profile of  $\log_{10}(S^2)$ , where  $S$  is vertical shear, from (a) observation, (b) SLH, (c) KPP, and (d)  $k$ - $\epsilon$  with 1-m vertical resolution.

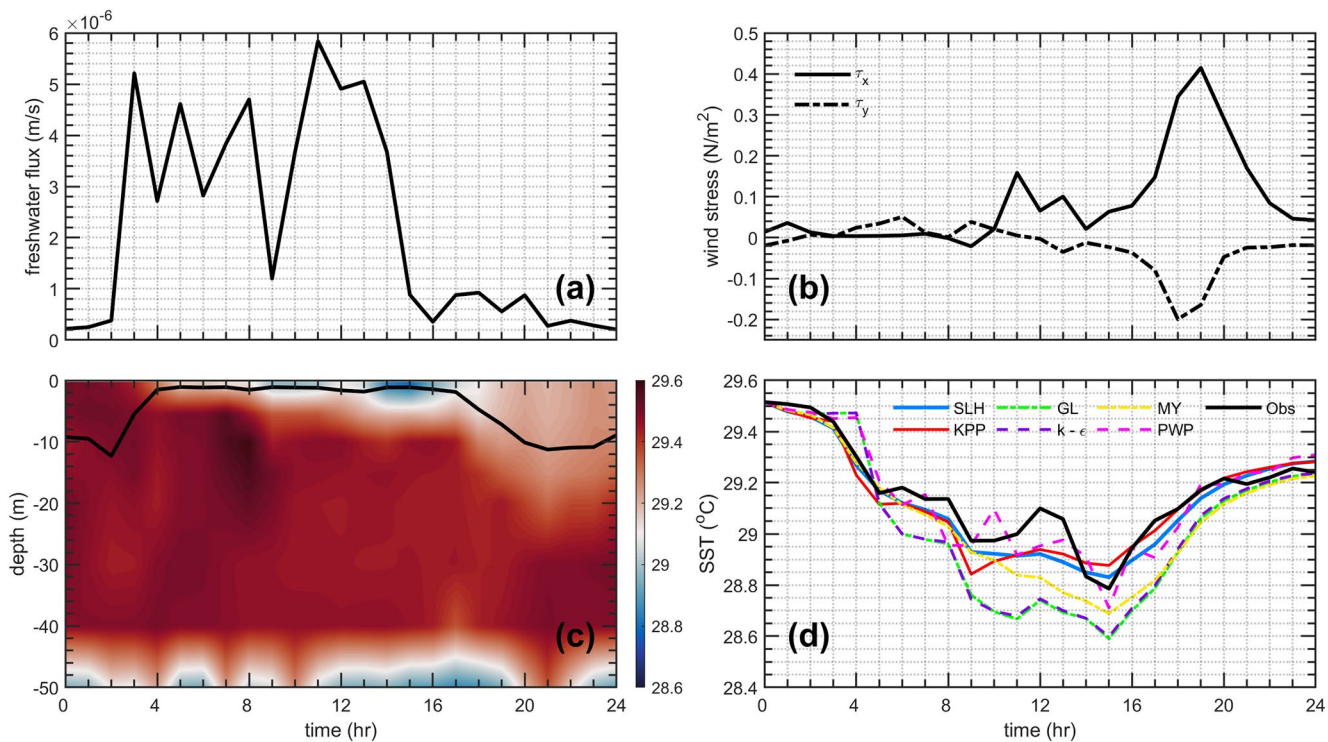


**Figure 6.** (a) Time series of surface freshwater flux (precipitation minus evaporation) in the cold pool event period from 09:00 27 October 2011 to 09:00 28 October 2011 GMT (14:00, 27 October 2011 to 14:00 28 October 2011 local standard time). Positive values indicate precipitation exceeding evaporation. (b) Time series of zonal (solid line) and meridional (dash-dotted line) wind stresses. (c) Temperature and the mixed layer depth (solid line) from observations. (d) Time series of sea surface temperature during the cold pool event on 27 October 2011 from observations (black line) and 1-D model simulations. Models are SLH, KPP, GL (generic length scale model), k- $\epsilon$ , MY, and PWP. Adapted from Pei et al. (2018).

observed during the cooling period. While processes that cause colder SSTs in second moment turbulence closure models are unknown, the weaker mixing below the mixed layer discussed in previous sections could be one possible reason. In this particular condition, the mixing causes SST warming because of the warmer waters below the shallow mixed layer, and thus weaker mixing may result in SSTs colder than observed.

By using validated 1-D ocean model simulations, processes controlling SST variations associated with cold pool events are further investigated (Pei et al., 2018). It is found that heavy precipitation causes not only the shallow mixed layer due to strong salinity stratification but also significant cooling due to the cold rainwater temperature. Also, gradual recovery of SST after its minimum is caused by the mixing of warm waters from below, rather than surface heat fluxes (Pei et al., 2018), suggesting that the accurate representation of vertical mixing (entrainment) under cold pool conditions is crucial for SST simulations.

### 3.2. Ocean General Circulation Model Simulations

The improved MOM5 which includes high resolution GOTM described in Section 2 is tested based on the comparison with observations. Using a previous version of MOM5 (before the implementation of GOTM), the large impact of vertical resolution near the surface on the simulation of diurnal cycle SST is demonstrated based on model simulations with the KPP mixing scheme and their comparison with the DYNAMO data (Ge et al., 2017). In the study of Ge et al. (2017), the model has been integrated from 1 September to 31 December 2011 with initial conditions taken from the oceanic state of the Climate Forecast System Reanalysis Version 2 (CFSv2; Saha et al., 2010, 2014) to compare with the DYNAMO observations. Using the improved MOM5, the same model simulations have been conducted to evaluate the model performance.

The horizontal resolution of the model is  $0.5^\circ$  in the zonal direction and varies in the meridional direction in which the grid spacing is  $0.25^\circ$  between  $10^\circ\text{S}$  and  $10^\circ\text{N}$ , gradually increasing poleward to  $0.5^\circ$  at  $30^\circ\text{S}$  and  $30^\circ\text{N}$  and fixed beyond. There are 50-layers in the vertical direction. As described in Section 2, the vertical

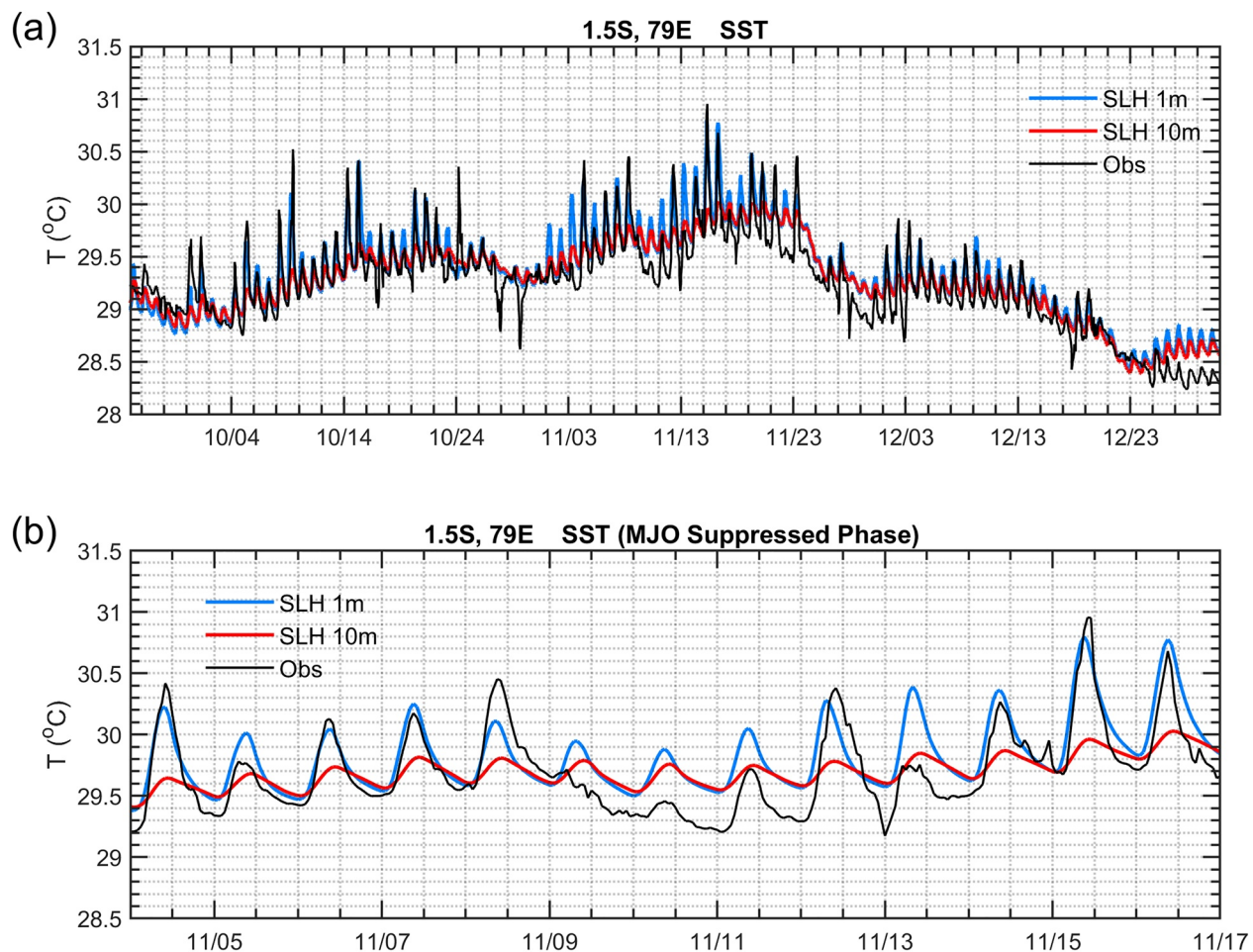


**Figure 7.** (a) Time series of SST at 1.5°S, 79°E during September 26–December 31 simulated by MOM5 with 1-m (blue line) and 10-m (red line) vertical resolutions in the upper 10 m and from observations (black line). The initial condition is derived from CFSv2. (b) Same as the upper panel except for the period 4–17 November during the suppressed phase of the MJO.

resolution of 1 m is used in the upper 10 m. To examine the impact of vertical resolution on SSTs for the new version of MOM5, the model with the 10-m vertical resolution near the surface is also integrated. The model is driven by hourly atmospheric forcing created by Ge et al. (2017) which is based on the 1-h outputs from CFSv2 and the Modern-Era Retrospective Analysis for Research and Applications (MERRA; Rienecker et al., 2011).

### 3.2.1. Intraseasonal and Diurnal SST Variations

Figure 7 shows the time series of SST during DYNAMO from the improved MOM5 with different vertical resolutions in the upper 10 m and observations. Here the model simulation with 1 m (10 m) resolution of upper 10 m is referred to as 1M (10M) simulation. The SLH scheme is used for the vertical mixing. Because of the high vertical resolution, both diurnal and intraseasonal variations are simulated by the model very well (Figure 7a). In particular, the amplitude of diurnal warming during the suppressed phase of the MJO is well reproduced by 1M simulation (Figure 7b). The amplitude of SST diurnal cycle in 10M simulation is much smaller, which is at least less than 30% of that in 1M simulation during the suppressed phase.

The 1M model simulations with the SLH scheme are compared with those with KPP (Figure 8). While both versions of the model are able to simulate diurnal and intraseasonal SST variations well, there are some significant differences. Consistent with 1-D model simulations, the amplitude of diurnal SST warming in the simulation with the KPP scheme is larger than that with the SLH scheme and observations. At 1.5°S, 79°E, the simulation with KPP generates SST warmer than SLH and observations from late November to

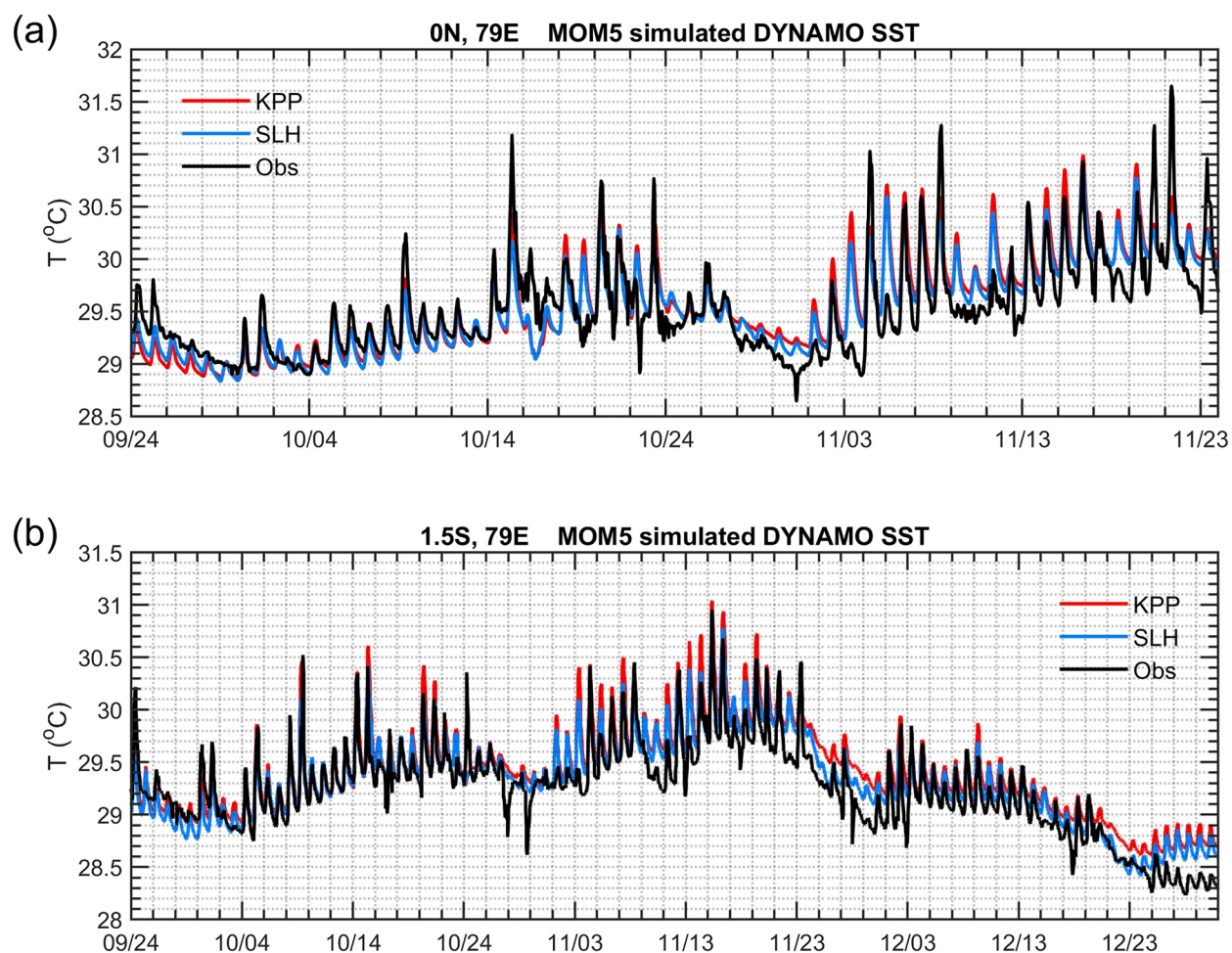


**Figure 8.** Time series of SST at (a)  $0^{\circ}$ ,  $79^{\circ}\text{E}$  and (b)  $1.5^{\circ}\text{S}$ ,  $79^{\circ}\text{E}$  during DYNAMO simulated by MOM5 with different mixing schemes (SLH and KPP) and observations. The vertical resolution in the upper 10 m of MOM5 simulations is 1 m. The initial condition is derived from CFSv2.

December when second and third MJO events during DYNAMO are observed (Figure 8b), which is also consistent with 1-D model simulations. This suggests that diurnal and intraseasonal SST variations during this period at these locations (at least  $1.5^{\circ}\text{S}$ ,  $79^{\circ}\text{E}$ ) are primarily controlled by 1-D processes, and thus 3-D model results confirm that the comparisons of 1-D models discussed in the previous section provide useful information for evaluating different mixing schemes.

### 3.2.2. Deep Cycle Turbulence

Deep cycle turbulence (DCT) is a diurnally oscillating turbulence that penetrates into a stratified shear layer below the mixed layer. DCT was first discovered in the eastern equatorial Pacific in 1980s by microstructure measurements (Gregg et al., 1985; Moum & Caldwell, 1985). Since then, it has often been observed in the eastern equatorial Pacific and eastern Atlantic Oceans where steady strong vertical shear is found due to the Equatorial Undercurrent which flows eastward below the westward flowing South Equatorial Current. Since its discovery, it has been extensively studied based mostly on the analysis of observational data (e.g., Inoue et al., 2012, 2019; Lien et al., 1995, 2008; Moum et al., 2009; Smyth & Moum, 2013; Smyth et al., 2017 and many others) and its importance for SST variations and climate variability has been suggested (e.g., Moum et al., 2013; Warner & Moum, 2019).

During DYNAMO, DCT is identified in the equatorial Indian Ocean for the first time (Pujiana et al., 2018). Based on the microstructure measurements in the central equatorial Indian Ocean during DYNAMO, Pujiana et al. (2018) suggested that turbulence penetration below the mixed layer during late November 2011 is associated with DCT driven by the vertical shear caused by the westerly winds associated with the MJO.

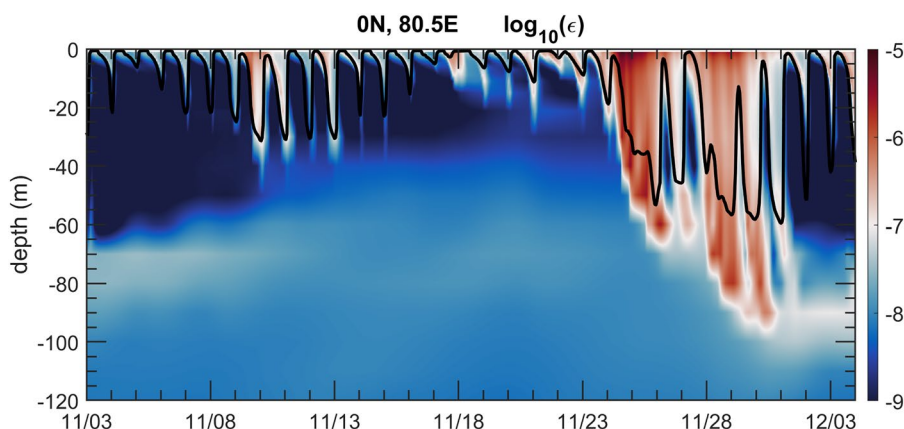


**Figure 9.** Time-depth contours of modeled  $\log_{10}(\epsilon)$  (shading), where  $\epsilon$  is the turbulence kinetic energy dissipation rate and mixed layer depth (black line) from 3 November to 3 December 2011 on the equator at 80.5°E. Adapted from Pei et al. (2020).

event (Moum et al., 2014). This DCT observed in the Indian Ocean, however, is somewhat thinner than that in the Pacific and Atlantic since the mixed layer is relatively deep during the active phase of the MJO.

Since a  $k$ - $\epsilon$  vertical mixing scheme is included in modified MOM5, the simulation of DCT is demonstrated through direct comparisons with turbulent dissipation derived from in-situ microstructure measurements including those during the DYNAMO measurements. The MOM5 has been integrated for the DYNAMO period using the  $k$ - $\epsilon$  scheme. Using the MOM5 simulation, DCT is identified for the first time in a global OGCM (Pei et al., 2020). Figure 9 shows the mixed layer depth and turbulent dissipation at the DYNAMO observation site ( $0^\circ$ , 80.5°E) during which DCT is observed in the equatorial Indian Ocean. In late November when westerly winds generate the deepening of the mixed layer, turbulent dissipation further penetrates below the mixed layer when the mixed layer deepening rate is reduced. The simulated DCT and its characteristics agree very well with observations (Figure 5 in the Pujiana et al., 2018). The characteristics of DCT in Pacific and Atlantic simulated by the same simulation are further discussed in Pei et al. (2020), which include zonal and meridional variations of DCT and modulation of DCT by tropical instability waves.

As a result of implementation of GOTM in MOM5, the ocean component of CFS is able to well represent the mixing associated with DCT. Hence, if the  $k$ - $\epsilon$  vertical mixing scheme is selected in CFS simulations, air-sea feedback processes associated with DCT could be investigated. While it is still unknown whether such feedback processes could impact the forecast skill, the accurate representation of physical processes in the upper ocean such as DCT will potentially reduce possible sources of model errors.

### 3.2.3. Impact of COARE3.5 Flux Algorithm on SST

The current operational version of CFS uses the bulk flux algorithm of Long (1984, 1986) with the thermal roughness length scale calculated by the method developed by Zeng et al. (1998) (referred to as the CFS flux algorithm hereafter). The CFS flux algorithm, which calculates latent and sensible heat fluxes using the model SST, is replaced with Coupled Ocean-Atmosphere Response Experiment (COARE) 3.5 algorithm (Edson et al., 2013; Fairall et al., 2003). The impact of COARE 3.5 algorithm implementation on the flux and SST is evaluated. The time series of latent heat flux and SST from the MOM5 simulations with COARE 3.5 and the CFS flux algorithm at DYNAMO mooring locations are shown in Figure 10a. While the difference in latent heat flux calculated by two algorithms is much smaller than the subseasonal fluctuation of latent heat flux, a significant difference of about 15–20 W/m<sup>2</sup> is occasionally found. The resultant SST change exceeds 0.2°C during the suppressed phase of the MJO in early mid-November which is significant in comparison to intraseasonal SST variability associated with the MJO. The spatial distribution of the difference during the MJO suppressed phase is shown in Figure 10c. A relatively large difference is found in the specific regions such as central Indian Ocean near the equator and northern part of Bay of Bengal, which exceeds 15 W/m<sup>2</sup>.

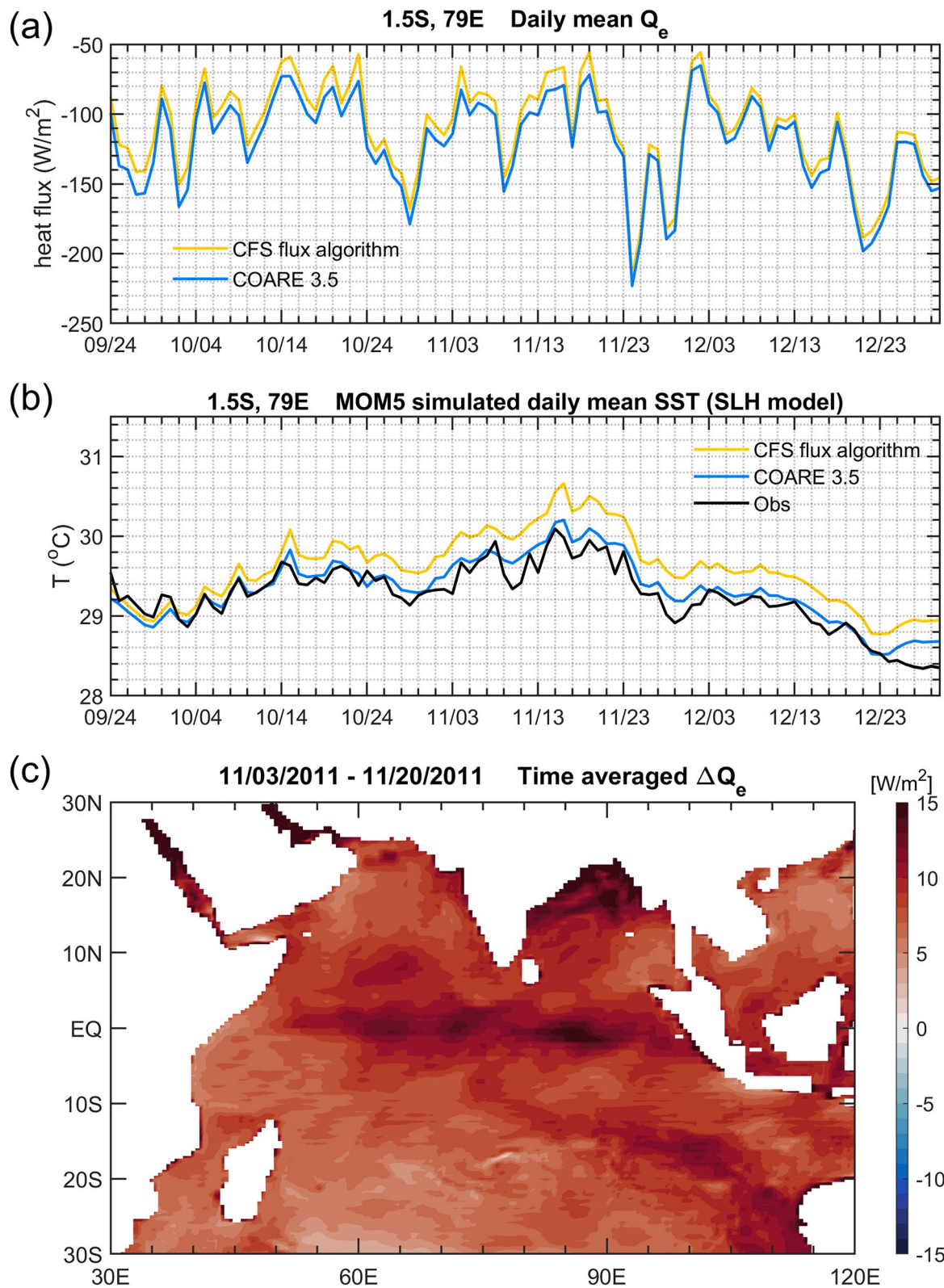


**Figure 10.** (a) Time series of daily mean latent heat flux  $Q_e$  and SST at 1.5°S, 79°E from the MOM5 simulations with COARE 3.5 (blue line) and the CFS flux algorithm (yellow line). (b) Same as (a) except for SST. (c) Difference in latent heat flux between MOM5 simulations with COARE 3.5 and the CFS flux algorithm. Positive values indicate larger latent heat fluxes of COARE 3.5.

### 3.3. CFS Simulations

In previous sections, several different improvements of the ocean component of CFS such as the increase of the vertical resolution and implementation of different mixing parameterizations are described. Among these changes, significant and systematic influences on MJO simulations are found for the improvement of the vertical resolution in the upper 10 m. Hence, in this section, the impact of vertical resolution on MJO simulations and prediction will be emphasized based on the simulations of MJO events observed during DYNAMO.

Previous studies suggest that the role of air-sea coupling in MJO development and propagation varies substantially from event to event, and that SST feedback plays a crucial role in the development of the second MJO event observed in late November to early December (Fu et al., 2015, 2017; Wang et al., 2015) while SST feedback has little effect during the event in October. Here, the MJO event occurred in late November simulated by CFS with the improvement of the ocean component is primarily discussed.

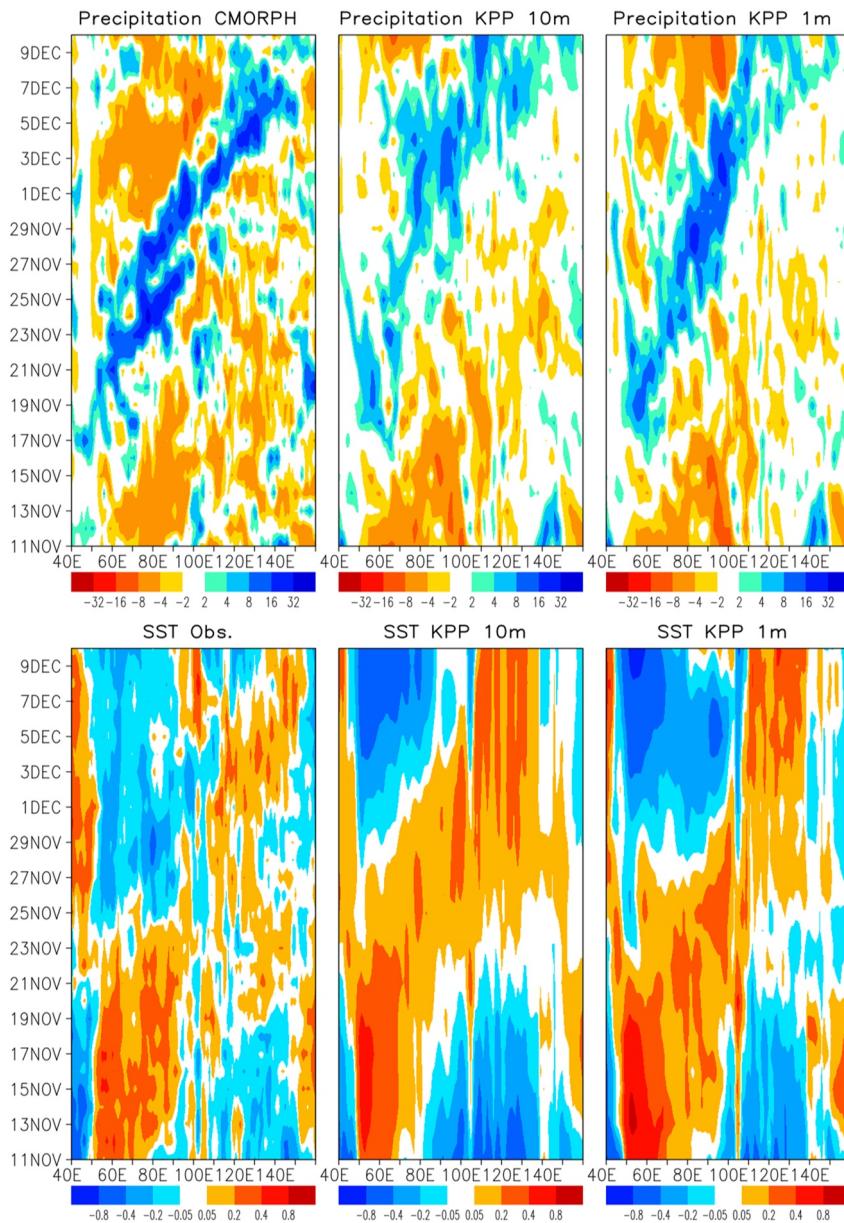
The CFS has been first integrated with the initial condition in early November to simulate the onset of MJO convection and its development in late November and the propagation during early December. As discussed in Section 3.2, the model version of the 1-m and 10-m vertical resolutions is used, and both KPP and SLH schemes are used for the CFS simulations. The CFS flux algorithm is used for all simulations. The model has been integrated for 30-day period with the initial conditions on November 7, 8, 9 and 10 derived from CFSv2. The time-lagged ensemble is calculated as the average of these four simulations with different initial conditions. The anomalies are calculated by subtracting the mean value at each longitude over the 30-day period of integration.

Figure 11 shows the forecast of precipitation anomaly associated with the MJO event using KPP scheme with the 1-m resolution (referred to as “CFSkpp\_r01”) and 10-m resolution (referred to as “CFSkpp\_r10”) and satellite-derived estimates from NOAA CPC Morphing Technique (CMORPH; Joyce et al., 2004). Both CFSkpp\_r01 and CFSkpp\_r10 are able to capture the initiation of convection between November 16 and 20 in the western Indian Ocean around 50°E–60°E, and the subsequent eastward propagation. It is found that the forecast with CFSkpp\_r01 which uses 1-m near-surface ocean vertical resolution produces more coherent propagation into the western Pacific than the CFSkpp\_r10. While observed precipitation anomaly is stronger than both CFS simulations, anomalous precipitation of CFSkpp\_r01 is much stronger than that in CFSkpp\_r10 and closer to observations. In particular, eastward propagation in the central and eastern Indian Ocean in 25 November–3 December 3 is well simulated in CFSkpp\_r01.

Sea surface temperature anomalies in the same simulations are also shown in Figure 11. The two simulations with different vertical resolutions in the ocean component are similar, and consistent with observations, with the forecast from CFSkpp\_r01 being more consistent in eastward propagation than that from CFSkpp\_r10, and is more similar to evolution of the observed SST anomalies. For example, during the MJO propagation in late November to early December, positive east-west SST gradient as a result of negative anomalies in the west and positive anomalies in the east is found in observations and CFS kpp01, but such prominent zonal SST gradient is not clear in CFSkpp\_r10.

Figure 12 shows the same CFS simulations but using the SLH parameterization in the ocean component (referred to as “CFSSlh\_r01” and “CFSSlh\_r10”). Most results are consistent with those with the KPP scheme. In particular, there is a clear difference between CFSSlh\_r01 and CFSSlh\_r10, which confirms the significant impact on the vertical resolution of the ocean component near the surface on MJO simulations. While both CFSSlh\_r01 and CFS kpp01 are able to simulate convection onset and subsequent propagation over the Indian Ocean reasonably well, the propagation in the Maritime Continent in CFSSlh\_r01 is slightly more consistent with the observations where coherent propagation is found up to around 120°E in CFSSlh\_r01. While such difference based on this MJO event cannot be used to rank these models, the result at least suggests that SST difference caused by different parameterizations could affect the characteristics of the simulated MJO. It should be noted that the two distinctive wave-like features in late November which are similar to observations are evident in CFSSlh\_r10, but the reason for this difference in the simulations is unknown.

To further confirm the impact of the vertical resolution on MJO simulations, the model simulations with different initial conditions which span from late October to the end of November have been conducted.



**Figure 11.** Upper panels: November 11 to December 10, 2011 rainfall (mm/day) anomaly from observations (left panel), simulations with CFSkpp\_r10 (middle panel, see text for the detail), and simulations from CFSkpp\_r01 (upper right panel). Anomalies are taken as the differences between the total fields and the average from November 11 to December 10, 2011. Lower panels: Same as upper panels except for SST.

Four-member (time-lagged) ensembles are calculated for each initial date. Since the model is integrated for 30-day period, the forecast up to 30 days can be examined. These MJO simulations by CFS with the 1-m vertical resolution reveal the right timing of convection onset and following coherent eastward propagation up to around 20-day forecast time, and the eastward propagation is becoming unclear for the forecast period longer than 25 days. Figure 13 shows the 19-day forecast for the period of early November to early December. The onset of MJO convection and subsequent eastward propagation are captured reasonably well in CFSslh\_r01. The model skill to simulate the MJO is reduced in CFSslh\_r10 in which the amplitude is much smaller than observations and CFSslh\_r01, and the eastward propagation is less coherent. A similar difference between simulations with 1- and 10-m vertical resolutions is found for CFS with the KPP scheme (not shown).

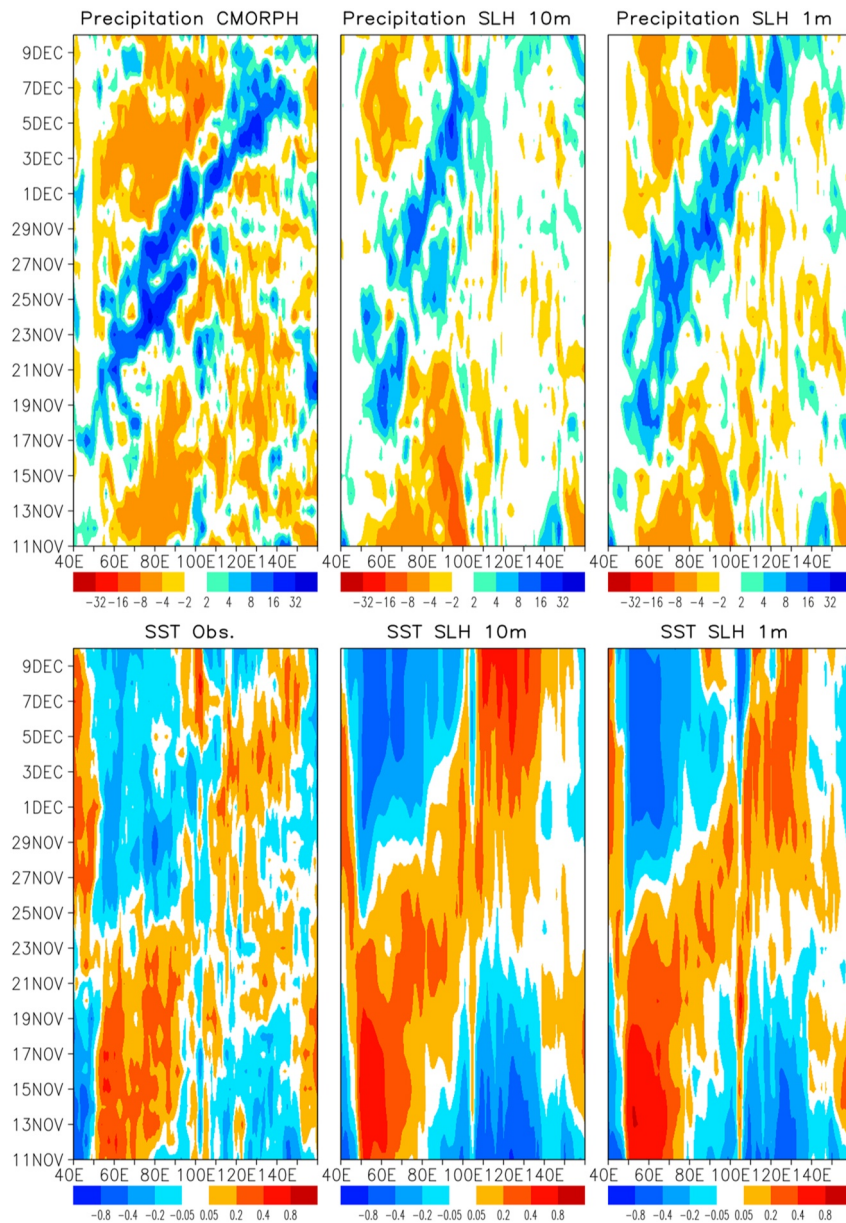


**Figure 12.** Same as Figure 11 except for simulations with SLH mixing parameterization.

It should be noted that the MJO propagation speed in all CFS simulations shown in Figures 11–13 is slower than the observed, which is consistent with previous studies (e.g., Weaver et al., 2011). Hence, the improvement of ocean component does not affect the propagation speed, suggesting that the slower propagation speed may be attributed to the deficiency in the atmospheric component of CFS.

In summary, a number of CFS simulations for the MJO event during DYNAMO demonstrate a significant difference of the model skill for the simulation between CFS with the 1-m and 10-m resolutions near the surface in the ocean component. The MJO simulated by CFS with 1-m resolution has more coherent eastward propagation, and the amplitude of anomalous precipitation is more realistic than those simulated by the model with 10-m resolution. This difference is clearly evident for both models with KPP and SLH mixing parameterizations.

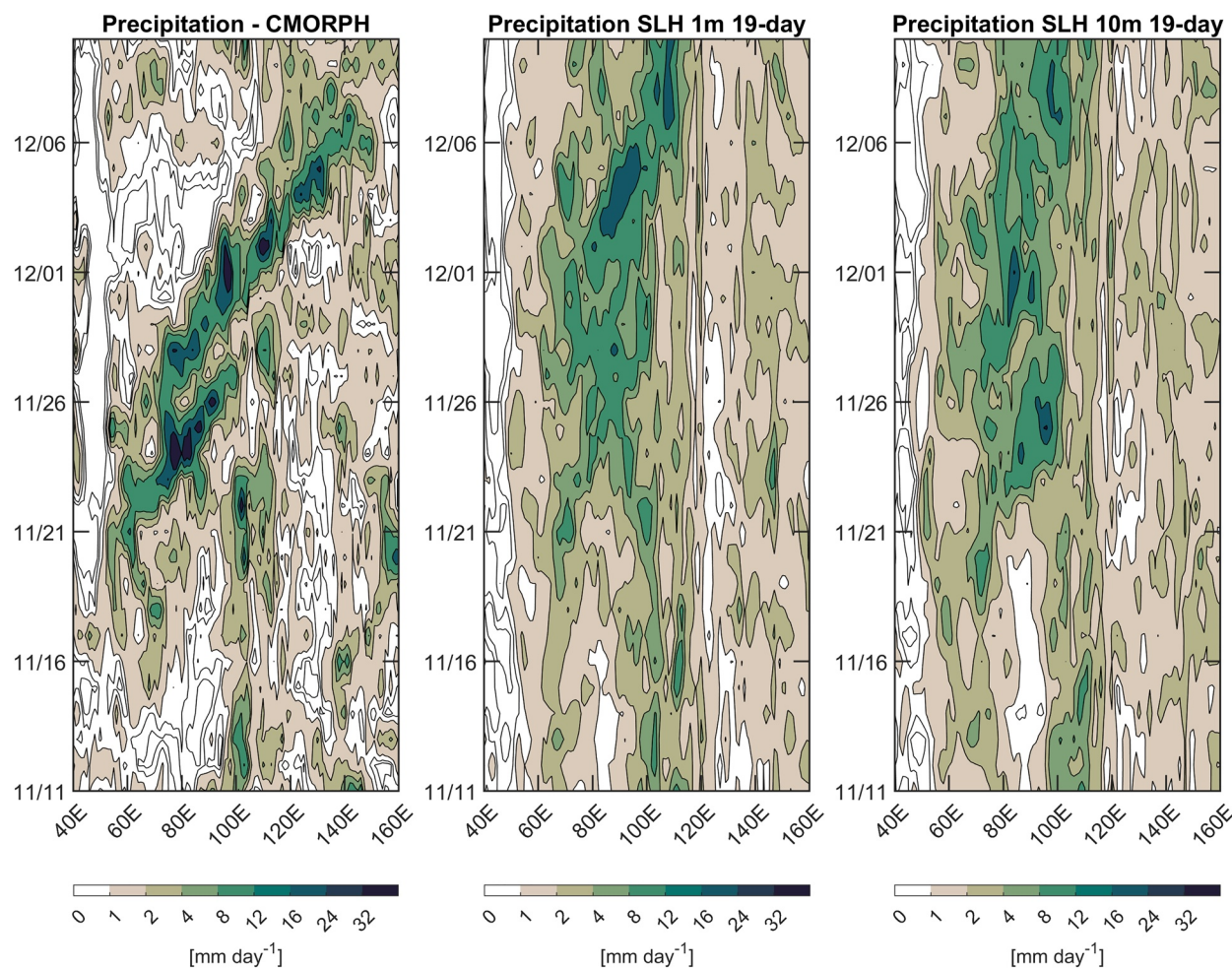


**Figure 13.** Precipitation (mm/day) averaged over  $10^{\circ}\text{N}$ – $10^{\circ}\text{S}$  estimated by CMORPH (left panel), its forecast at 19-day time by CFSslh\_r01 (middle panel), and CFSslh\_r10 (right panel).

#### 4. Summary and Discussion

In 2015, NOAA made an announcement to support Climate Process Teams (CPTs), which focus on improving simulations of the MJO by NOAA's global forecast models using the observational data collected during the recent field campaign. Our CPT project specifically focuses on the improvement of ocean component of NOAA CFS for realistically simulating the MJO development and propagation especially over the Indian Ocean. The results of our CPT project are summarized in this paper.

The major observational data used in this study are those collected in the recent field campaign: Dynamics of the MJO (DYNAMO) in the tropical Indian Ocean. In particular, the data for the DYNAMO Intensive Observing Period (IOP) in fall/winter 2011, during which three well-defined MJO convection propagated over the tropical Indian Ocean, are primarily used to validate the model simulations.

The current operational version of CFS uses MOM4 with KPP upper ocean mixing scheme in the ocean component, and the vertical resolution near the surface is about 10 m. First, MOM4 has been replaced with MOM5 before changing the ocean component. Given the potential importance of diurnal SST variation and the evolution of MJO-induced near surface currents for the MJO simulations, the primary changes of the ocean component in this project include the increase of the vertical resolution to 1-m in the upper ocean and the implementation of General Ocean Turbulence Model (GOTM) which contains several different mixing schemes. The mixing parameterization developed based on ocean measurements in the tropical Pacific warm pool (SLH scheme: Soloviev et al., 2001) has been added to GOTM with some modifications.

The improved GOTM has been evaluated first in 1-D modeling framework based on the comparison with the DYNAMO data. 1-D models with several different mixing schemes are integrated with accurate surface air-sea fluxes estimated from DYNAMO measurements. Overall, all 1-D models are able to simulate SST variations associated with the MJO reasonably well. In particular, it is found that the 1-m resolution of upper 10 m is sufficient to realistically simulate the large diurnal warming of SST during the suppressed phase of the MJO which is observed by DYNAMO moorings. A significant difference between different mixing schemes in simulating the SST diurnal cycle is evident. For example, second moment turbulence closure models overestimate the amplitude of observed SST diurnal warming due primarily to too weak mixing below the mixed layer. The weak mixing in second moment turbulence closure models is further confirmed by the simulation of vertical shear and the ocean response to atmospheric cold pools.

The ocean component is then evaluated by simulations of improved MOM5 with GOTM based on the comparison with the observational data. Consistent with 1-D model simulations, the improved MOM5 is able to simulate SST variations well, including the large diurnal warming during the MJO suppressed phase and rapid cooling during the MJO active phase. It is further demonstrated that the improved MOM5 is able to simulate deep cycle turbulence in the equatorial oceans, including that observed in the central equatorial Indian Ocean during DYNAMO.

A number of CFS simulations have been conducted with initial conditions of different dates from late October to the end of November. The period of the simulations covers the convection onset and subsequent eastward propagation of second MJO event during DYNAMO. Consistent with previous studies, which suggest the important role of air-sea coupling in this event, changes in ocean component of CFS have a significant impact on the MJO simulations. In particular, the vertical resolution of upper 10-m strongly influences the model skill to predict the propagation of this MJO. It is shown that the simulated MJO by CFS with the 1-m vertical resolution of upper ocean is more similar to observations than that with the 10-m resolution. Compared to CFS with the 10-m resolution, the 1-m resolution version is able to simulate more coherent eastward propagation and the amplitude closer to observations.

While the difference in upper ocean vertical mixing schemes affects the MJO characteristics for this particular event, it is not possible to rank these schemes in terms of MJO prediction skills. As suggested in recent studies (e.g., Fu et al., 2015, 2017), the role of air-sea coupling in the MJO varies substantially from event to event. Hence it is likely that the impact of ocean component improvement on MJO simulations also varies from event to event. It is possible that ocean vertical resolution demonstrated to be important for simulation of the MJO during DYNAMO might not impact the prediction skill in some other events. The impact could be different in MJO events which occur in other locations and different seasons. While the comprehensive data from the DYNAMO field campaign, which was specifically designed for monitoring the MJO, are available and thus this study focused on the MJO over the Indian Ocean during DYNAMO, it is necessary in future to test the improved CFS (or future version of prediction system) in many other MJO events using the data from current and future field campaigns. Such data from international field campaigns are becoming available in recent years. For example, field phase of Years of the Maritime Continent (YMC; Yoneyama & Zhang, 2020), which provides both oceanic and atmospheric data over the Maritime Continent (MC), will be completed in the next few years. The YMC data should be particularly useful for model-data integration in terms of MJO simulations, since many coupled prediction systems still have problems in simulating the MJO propagation over the MC region.

The role of air-sea interaction could also depend on the atmospheric component of prediction system. For example, previous studies suggest that different cumulus convection schemes such as RAS (Relaxed Arakawa-Schubert) and SAS (Simplified Arakawa-Schubert) cause significant differences in skills of MJO simulations by GFS forced with observed SSTs and they are also sensitive to SST products used for the simulations (Wang et al., 2015). Hence it is possible that atmospheric response to diurnal and intraseasonal SST fluctuations could be also different for different atmospheric components. Accordingly, the improvement of atmospheric component in coupled prediction system is necessary to further quantify the impact of ocean component improvement on the prediction skill of the MJO. Yet, to improve the atmospheric component, uncertainty caused by the deficiency of ocean component needs to be identified and such deficiency needs to be remedied to identify major atmospheric processes that influence the MJO prediction skills. To this end, this study, which has improved the diurnal and intraseasonal variations of SST using the high vertical

resolution of ocean component and identified its impact on MJO simulations, at least provides useful information. For example, with the improvement of oceanic processes in the system, poor skills of the MJO prediction in some cases cannot be largely attributed to the ocean component. The improvement of ocean component thus will help isolate the important atmospheric processes if not represented well in the coupled system.

One of the major on-going efforts in modeling communities supported by NOAA and other agencies is the development of next generation coupled prediction system: Unified Forecast System (UFS). Currently, the UFS is planned to be used for NOAA's operational forecast within a few years by replacing the current operational version of CFS. The atmospheric component of UFS is FV3GFS which uses existing GFS v14 physics with the GFDL microphysics scheme. Most model physics in FV3GFS are similar to the current version of GFS although there are substantial improvements in its numerics (resolutions, grid configurations etc.). Hence, the impact of the representation of upper ocean processes in MJO simulation identified in this study could be similar in UFS. Accordingly, results from our project will hopefully provide useful information for current effort of UFS development and improvement. The evaluation of upper ocean processes relevant to the MJO simulation in the ocean component of UFS: Modular Ocean Model version 6 (MOM6) is one of our current and future researches.

## Data Availability Statement

The DYNAMO mooring measurements used are obtained from <http://www.eol.ucar.edu/projects/dynamo>. CMORPH precipitation data are obtained from NOAA NWS/CPC at [https://www.cpc.ncep.noaa.gov/products/janowiak/cmorph\\_description.html](https://www.cpc.ncep.noaa.gov/products/janowiak/cmorph_description.html). TMI SST data are obtained from the Remote Sensing System at <http://www.remss.com/missions/tmi>. CFSv2 data can be accessed at <https://www.ncdc.noaa.gov/data-access/model-data/model-datasets/climate-forecast-system-version2-cfsv2>. MERRA data can be found at <https://gmao.gsfc.nasa.gov/reanalysis/MERRA/>. Model output data required to reconstruct the figures in this paper and the model code of SLH parameterization are publicly available at <https://doi.org/10.6084/m9.figshare.14780115>. Colormap used to produce some of the figures is obtained from Thyng et al. (2016).

## Acknowledgments

This research was supported by NOAA Grant NA15OAR431074. Computing resources were provided partly by the HPC systems at the Texas A&M University (College Station and Corpus Christi) and the Climate Simulation Laboratory at NCAR's Computational and Information Systems Laboratory, sponsored by the National Science Foundation. TS and SP are supported by DOD Grant W911NF-20-1-0309. TS is also supported by NSF Grant OCE-1658218 and NOAA Grant NA17OAR4310256. Constructive comments by two anonymous reviewers are gratefully acknowledged.

## References

- Bellenger, H., Takayabu, Y. N., Ushiyama, T., & Yoneyama, K. (2010). Role of diurnal warm layers in the diurnal cycle of convection over the tropical Indian Ocean during MISMO. *138. Monthly Weather Review*, 138, 2426–2433. <https://doi.org/10.1175/2010MWR3249.1>
- Bernie, D., Guilyardi, E., Madec, G., Slingo, J., & Woolnough, S. (2007). Impact of resolving the diurnal cycle in an ocean-atmosphere GCM. Part 1: A diurnally forced OGCM. *Climate Dynamics*, 29, 575–590. <https://doi.org/10.1007/s00382-007-0249-6>
- Bernie, D. J., Woolnough, S. J., Slingo, J. M., & Guilyardi, E. (2005). Modeling diurnal and intraseasonal variability of the ocean mixed layer. *Journal of Climate*, 18, 1190–1202. <https://doi.org/10.1175/JCLI319.1>
- Bretherton, C. S., Ferrari, R., & Legg, S. (2004). Climate Process Teams: A new approach to improving climate models. *U.S. CLIVAR Variations*, 2(No. 1), 1–6.
- Burchard, H., & Bolding, K. (2001). Comparative Analysis of Four Second-Moment Turbulence Closure Models for the Oceanic Mixed Layer. *Journal of Physical Oceanography*, 31, 1943–1968. [https://doi.org/10.1175/1520-0485\(2001\)031<1943:caofsm>2.0.co;2](https://doi.org/10.1175/1520-0485(2001)031<1943:caofsm>2.0.co;2)
- Burchard, H., Bolding, K., & Villarreal, M. R. (1999). GOTM, a General Ocean Turbulence Model. Theory, implementation and test cases (Technical Report EUR 18745 EN). Ispra, Italy: European Commission.
- Canuto, V. M., Howard, A. Y., Dubovikov, M. S., & Dubovikov, M. S. (2001). Ocean Turbulence. Part I: One point closure model-momentum and heat vertical diffusivities. *Journal of Physical Oceanography*, 31, 1413–1426. [https://doi.org/10.1175/1520-0485\(2001\)031<1413:otpiop>2.0.co;2](https://doi.org/10.1175/1520-0485(2001)031<1413:otpiop>2.0.co;2)
- Chen, S. S., Kerns, B. W., Guy, N., Jorgensen, D. P., Delanoë, J., Viltard, N., et al. (2016). Aircraft observations of dry air, the ITCZ, convective cloud systems, and cold pools in MJO during DYNAMO. *Bulletin of the American Meteorological Society*, 97(3), 405–423. <https://doi.org/10.1175/bams-d-13-00196.1>
- Cheng, Y., Canuto, V. M., & Howard, A. M. (2002). An Improved Model for the Turbulent PBL. *Journal of the Atmospheric Sciences*, 59, 1550–1565. [https://doi.org/10.1175/1520-0469\(2002\)059<1550:aimftt>2.0.co;2](https://doi.org/10.1175/1520-0469(2002)059<1550:aimftt>2.0.co;2)
- Chi, N.-H., Lien, R.-C., & D'Asaro, E. A. (2021). The mixed layer salinity budget in the central equatorial Indian Ocean. *Journal of Geophysical Research*, 126. <https://doi.org/10.1029/2021JC017280>
- Chi, N.-H., Lien, R.-C., D'Asaro, E. A., & Ma, B. B. (2014). The surface mixed layer heat budget from mooring observations in the central Indian Ocean during Madden-Julian Oscillation events. *Journal of Geophysical Research: Ocean*, 119, 4638–4652. <https://doi.org/10.1002/2014jc010192>
- de Szoëke, S. P., & Edson, J. B. (2017). Intraseasonal air-sea interaction and convection observed in DYNAMO/CINDY/AMIE and TOGA COARE. *The global monsoon system: Research and forecast* (pp. 349–364). Singapore: World Scientific. [https://doi.org/10.1142/9789813200913\\_0028](https://doi.org/10.1142/9789813200913_0028)
- DeMott, C. A., Klingaman, N. P., & Woolnough, S. J. (2015). Atmosphere-ocean coupled processes in the Madden-Julian oscillation. *Reviews of Geophysics*, 53, 1099–1154. <https://doi.org/10.1002/2014RG000478>

- Edson, J. B., Jampana, V., Weller, R. A., Bigorre, S. P., Plueddemann, A. J., Fairall, C. W., et al. (2013) On the exchange of momentum over the open ocean. *J. Phys. Oceanogr.*, 43, 1589–1610. <https://doi.org/10.1175/JPO-D-12-0173.1>
- Fairall, C. W., Bradley, E. F., Hare, J. E., Grachev, A. A., & Edson, J. B. (2003). Bulk parameterization of air-sea fluxes: Updates and verification for the COARE algorithm. *Journal of Climate*, 16, 571–591. [https://doi.org/10.1175/1520-0442\(2003\)016<0571:NPAAFO>2.0.CO;2](https://doi.org/10.1175/1520-0442(2003)016<0571:NPAAFO>2.0.CO;2)
- Feng, Z., Hagos, S., Rowe, A. K., Burleyson, C. D., Martini, M. N., & de Szoeke, S. P. (2015). Mechanisms of convective cloud organization by cold pools over tropical warm ocean during the AMIE/DYNAMO field campaign. *Journal of Advances in Modeling Earth Systems*, 7(2), 357–381. <https://doi.org/10.1002/2014MS000384>
- Flatau, M., Flatau, P. J., Phoebus, P., & Niiler, P. P. (1997). The feedback between equatorial convection and local radiative and evaporative processes: The implication for intraseasonal oscillations. *Journal of the Atmospheric Sciences*, 54, 2373–2386. [https://doi.org/10.1175/1520-0469\(1997\)054<2373:TFBEC>2.0.co;2](https://doi.org/10.1175/1520-0469(1997)054<2373:TFBEC>2.0.co;2)
- Fu, J.-X., Wang, W., Shinoda, T., Ren, H.-L., & Jia, X. L. (2017). Toward understanding the diverse impacts of air-sea interactions on MJO simulations. *JGR-Oceans*, 122(11), 8855–8875. <https://doi.org/10.1002/2017jc013187>
- Fu, X., Wang, W., Lee, J.-Y., Wang, B., Kikuchi, K., Xu, J., et al. (2015). Distinctive roles of air-sea coupling on different MJO events: A new perspective revealed from the DYNAMO/CINDY field campaign, 143. *Mon. Wea. Rev.*, 143, 794–812. <https://doi.org/10.1175/MWR-D-14-00221.1>
- Ge, X., Wang, W., Kumar, A., & Zhang, Y. (2017). Importance of the vertical resolution in simulating SST diurnal and intraseasonal variability in an oceanic general circulation model. *Journal of Climate*, 30, 3963, 3978. <https://doi.org/10.1175/CLD-D-16-0689.1>
- Gottschalck, J., Roundy, P., Schreck, C., Vintzileos, A., & Zhang, C. (2013). Large-scale Atmospheric and Oceanic Conditions During the 2011–2012 DYNAMO Field Campaign. *Monthly Weather Review*, 141, 4173–4196. <https://doi.org/10.1175/mwr-d-13-00022.1>
- Gregg, M. C., Peters, H., Wesson, J. C., Oakey, N. S., & Shay, T. J. (1985). Intensive measurements of turbulence and shear in the equatorial undercurrent. *Nature*, 318(6042), 140–144. <https://doi.org/10.1038/318140a0>
- Huyer, A., Kosro, P. M., Lukas, R., & Hacker, P. (1997). Upper ocean thermohaline fields near 2°S, 156°E, during the tropical ocean-global atmosphere response experiment. *Journal of Geophysical Research*, 102(12), 12749–12784. <https://doi.org/10.1029/97jc00267>
- Inoue, R., Lien, R.-C., & Moum, J. N. (2012). Modulation of equatorial turbulence by a tropical instability wave. *Journal of Geophysical Research*, 117, C10009-n. <https://doi.org/10.1029/2011JC007767>
- Inoue, R., Lien, R.-C., Moum, J. N., Perez, R. C., & Gregg, M. C. (2019). Variations of equatorial shear, stratification, and turbulence within a tropical instability wave cycle. *Journal of Geophysical Research: Oceans*, 124, 1858–1875. <https://doi.org/10.1029/2018JC014480>
- Joyce, R. J., Janowiak, J. E., Arkin, P. A., & Xie, P. (2004). CMORPH: A method that produces global precipitation estimates from passive microwave and infrared data at high spatial and temporal resolution. *Journal of Hydrometeorology*, 5, 487–503. [https://doi.org/10.1175/1525-7541\(2004\)005<0487:camptg>2.0.co;2](https://doi.org/10.1175/1525-7541(2004)005<0487:camptg>2.0.co;2)
- Katsaros, K. B., & Soloviev, A. (2004). Vanishing horizontal sea surface temperature gradients at low wind speeds. *Boundary-Layer Meteorology*, 112, 381–396. <https://doi.org/10.1023/b:boun.0000027905.90989.b2>
- Katsaros, K. B., Soloviev, A., Weisberg, R. H., & Luther, M. E. (2005). Reduced Horizontal Sea Surface Temperature Gradients Under Conditions of Clear Skies and Weak Winds. *Boundary-Layer Meteorology*, 116(2), 175–185. <https://doi.org/10.1007/s10546-004-2421-4>
- Large, W. G., McWilliams, J. C., & Doney, S. C. (1994). Oceanic vertical mixing: Review and a model with a nonlocal boundary layer parameterization. *Reviews of Geophysics*, 32, 363–403. <https://doi.org/10.1029/94RG01872>
- Legg, S., Briegleb, B., Chang, Y., Chassignet, E. P., Danabasoglu, G., Ezer, T., et al. (2009). Improving oceanic overflow representation in climate models: The Gravity Current Entrainment Climate Process Team. *Bulletin of the American Meteorological Society*, 90, 657–670. <https://doi.org/10.1175/2008bams2667.1>
- Li, Y., Han, W., Shinoda, T., Wang, C., Lien, R.-C., Moum, J. N., & Wang, J. W. (2013). Effects of solar radiation diurnal cycle on the tropical Indian Ocean mixed layer variability during wintertime Madden-Julian oscillation events. *Journal of Geophysical Research: Oceans*, 118, 4945–4964. <https://doi.org/10.1002/jgrc.20395>
- Lien, R.-C., Caldwell, D. R., Gregg, M. C., & Moum, J. N. (1995). Turbulence variability at the equator in the central Pacific at the beginning of the 1991–1993 El Niño. *Journal of Geophysical Research*, 100(C4), 6881–6898. <https://doi.org/10.1029/94jc03312>
- Lien, R.-C., D'Asaro, E., & Menkes, C. (2008). Modulation of equatorial turbulence by tropical instability waves. *Geophysical Research Letters*, 35, L24607. <https://doi.org/10.1029/2008GL035860>
- Long, P. J. (1984). An general unified similarity theory for the calculation of turbulent fluxes in the numerical weather prediction models for unstable condition. *Office Note* (Vol. 302, p. 30). Department of Commerce, NOAA, NWS, National Meteorological Center.
- Long, P. J. (1986). An economical and compatible scheme for parameterizing the stable surface layer in the medium-range forecast model. *Office Note* (Vol. 321, p. 24). U.S. Department of Commerce, NOAA, NWS, National Meteorological Center.
- MacKinnon, J., Zhao, Z., Whalen, C. B., Waterhouse, A. F., Trossman, D. S., Sun, O. M., et al. (2017). Climate process team on internal-wave driven ocean mixing. *Bulletin of the American Meteorological Society*, 98(11), 2429–2454. <https://doi.org/10.1175/BAMS-D-16-0030.1>
- Madden, R. A., & Julian, P. R. (1972). Description of global-scale circulation cells in the tropics with a 40–50 day period. *Journal of the Atmospheric Sciences*, 29, 1109–1123. [https://doi.org/10.1175/1520-046910.1175/1520-0469\(1972\)029<1109:dogsc>2.0.co;2.197209<11092](https://doi.org/10.1175/1520-046910.1175/1520-0469(1972)029<1109:dogsc>2.0.co;2.197209<11092)
- Mellor, G. L., & Yamada, T. (1982). Development of a turbulence closure model for geophysical fluid problems. *Reviews of Geophysics*, 20, 851–875. <https://doi.org/10.1029/rg020i004p00851>
- Moum, J. N., & Caldwell, D. R. (1985). Local influences on shear-flow turbulence in the equatorial ocean. *Science*, 230(4723), 315–316. <https://doi.org/10.1126/science.230.4723.315>
- Moum, J. N., de Szoeke, S. P., Smyth, W. D., Edson, J. B., DeWitt, H. L., Moulin, A. J., et al. (2014). Air-sea interactions from westerly wind bursts during the November 2011 MJO in the Indian Ocean. *Bulletin of the American Meteorological Society*, 95, 1185–1199. <https://doi.org/10.1175/BAMS-D-12-00225.1>
- Moum, J. N., Lien, R.-C., Perlin, A., Nash, J. D., Gregg, M. C., & Wiles, P. J. (2009). Sea surface cooling at the equator by subsurface mixing in tropical instability waves. *Nature Geoscience*, 2(11), 761–765. <https://doi.org/10.1038/ngeo657>
- Moum, J. N., Perlin, A., Nash, J. D., & McPhaden, M. J. (2013). Seasonal sea surface cooling in the equatorial Pacific cold tongue controlled by ocean mixing. *Nature*, 500(7460), 64–67. <https://doi.org/10.1038/nature12363>
- Paulson, C. A., & Simpson, J. J. (1977). Irradiance measurements in the upper ocean. *Journal of Physical Oceanography*, 7(6), 952–956. [https://doi.org/10.1175/1520-0485\(1977\)007%3C0952:IMITUO%3E2.0.CO;2](https://doi.org/10.1175/1520-0485(1977)007%3C0952:IMITUO%3E2.0.CO;2)
- Pei, S., Shinoda, T., Soloviev, A., & Lien, R.-C. (2018). Upper ocean response to the atmospheric cold pools associated with the Madden-Julian oscillation. *Geophysical Research Letters*, 45, 5020–5029. <https://doi.org/10.1029/2018GL077825>
- Pei, S., Shinoda, T., Wang, W., & Lien, R.-C. (2020). Simulation of deep cycle turbulence by a global ocean general circulation model. *Geophysical Research Letters*, 47, e2020GL088384. <https://doi.org/10.1029/2020GL088384>

- Peters, H., Gregg, M. C., & Toole, J. M. (1988). On the parametrization of equatorial turbulence. *Journal of Geophysical Research*, 93, 1199–1218. <https://doi.org/10.1029/jc093ic02p01199>
- Price, J. F., Weller, R. A., & Pinkel, R. (1986). Diurnal cycling: Observations and models of the upper ocean response to diurnal heating, cooling, and wind mixing. *Journal of Geophysical Research*, 91(C7), 8411–8427. <https://doi.org/10.1029/JC091iC07p08411>
- Pujiana, K., Moum, J. N., & Smyth, W. D. (2018). The role of turbulence in redistributing upper-ocean heat, freshwater, and momentum in response to the MJO in the equatorial Indian Ocean. *Journal of Physical Oceanography*, 48(1), 197–220. <https://doi.org/10.1175/jpo-d-17-0146.1>
- Rienecker, M. M., Suarez, M. J., Gelaro, R., Todling, R., Bacmeister, J., Liu, E., et al. (2011) MERRA: NASA's Modern-Era retrospective analysis for research and applications, *Journal of Climate*, 24, 3624–3648. <https://doi.org/10.1175/JCLI-D-11-00015.1>
- Rodi, W. (1987). Examples of calculation methods for flow and mixing in stratified fluids. *Journal of Geophysical Research: Oceans*, 92(C5), 5305–5328. <https://doi.org/10.1029/jco92ic05p05305>
- Saha, S., Moorhtsi, S., au, X., Wang, J., Nadiga, S., Tripp, P., et al. (2014). The NCEP climate forecast system version 2. *Journal of Climate*, 27, 2185–2208. <https://doi.org/10.1175/JCLI-D-12-00823.1>
- Saha, S., Moorhtsi, S., Pan, H.-L., Wu, X., Wang, J., Nadiga, S., et al. (2010). The NCEP climate forecast system reanalysis. *Bulletin of the American Meteorological Society*, 91, 1015–1058. <https://doi.org/10.1175/2010BAMS3001.1>
- Seo, H., Subramanian, A. C., Miller, A. J., & Cavanaugh, N. R. (2014). Coupled impacts of the diurnal cycle of sea surface temperature on the Madden-Julian Oscillation. *Journal of Climate*, 27, 8422–8443. <https://doi.org/10.1175/JCLI-D-14-00141.1>
- Shinoda, T., HanHan, W. L., Zamudio, R.-C., & Katsumata, M. (2017). Remote ocean response to the Madden-Julian oscillation during the DYNAMO field campaign: Impact on Somali current system and the Seychelles-Chagos Thermocline Ridge. *Atmosphere*, 8, 171. <https://doi.org/10.3390/atmos8090171>
- Shinoda, T. (2005). Impact of the diurnal cycle of solar radiation on intraseasonal SST variability in the western equatorial Pacific. *Journal of Climate*, 18, 2628–2636. <https://doi.org/10.1175/JCLI3432.1>
- Shinoda, T., Han, W., Jensen, T., Zamudio, L., Metzger, E. J., & Lien, R.-C. (2016). Impact of the Madden-Julian oscillation on the Indonesian throughflow in Makassar strait during the CINDY/DYNAMO field campaign. *Journal of Climate*, 29, 6085–6108. <https://doi.org/10.1175/jcli-d-15-0711.1>
- Shinoda, T., & Hendon, H. H. (1998). Mixed layer modeling of intraseasonal variability in the tropical western Pacific and Indian Oceans. *Journal of Climate*, 11, 2668–2685. [https://doi.org/10.1175/1520-0442\(1998\)011<2668:MLMOIV>2.0.co;2](https://doi.org/10.1175/1520-0442(1998)011<2668:MLMOIV>2.0.co;2)
- Shinoda, T., & Hendon, H. H. (2001). Upper ocean heat budget in response to the Madden-Julian Oscillation in the western equatorial Pacific. *Journal of Climate*, 14, 4147–4165. [https://doi.org/10.1175/1520-0442\(2001\)014<4147:uoohbir>2.0.co;2](https://doi.org/10.1175/1520-0442(2001)014<4147:uoohbir>2.0.co;2)
- Shinoda, T., Hendon, H. H., & Glick, J. (1998). Intraseasonal variability of surface fluxes and sea surface temperature in the tropical western Pacific and Indian Oceans. *Journal of Climate*, 11, 1685–1702. [https://doi.org/10.1175/1520-0442\(1998\)011<1685:IVOSFA>2.0.co;2](https://doi.org/10.1175/1520-0442(1998)011<1685:IVOSFA>2.0.co;2)
- Shinoda, T., Jensen, T. G., Flatau, M., Chen, S., Han, W., & Wang, C. (2013). Large-scale oceanic variability associated with the Madden-Julian oscillation during the CINDY/DYNAMO field campaign from satellite observations. *Remote Sensing*, 5, 2072–2092. <https://doi.org/10.3390/rs5052072>
- Smyth, W. D., & Moum, J. N. (2013). Marginal instability and deep cycle turbulence in the eastern equatorial Pacific Ocean. *Geophysical Research Letters*, 40, 6181–6185. <https://doi.org/10.1002/2013GL058403>
- Smyth, W. D., Pham, H. T., Moum, J. N., & Sakar, S. (2017). Pulsating turbulence in a marginally unstable stratified shearflow. *Journal of Fluid Mechanics*, 822, 327–341. <https://doi.org/10.1017/jfm.2017.283>
- Soloviev, A., Edson, J., McGillivray, S., Schluessel, P., & Wan-ninkof, R. (2002). Fine thermohaline structure and gas-exchange in the near-surface layer of the ocean during GasEx-98. In M. A. Donelan, W. M. Drennan, E. S. Saltzman & R. Wanninkhof (Eds.), *Gas Transfer at Water Surfaces. Geophysical Monograph Series* (Vol. 127, pp. 181–185). Washington, DC: AGU.
- Soloviev, A., & Lukas, R. (1997). Sharp frontal interfaces in near-surface layer of the ocean in the western Pacific warm pool. *Journal of Physical Oceanography*, 27, 999–1017. [https://doi.org/10.1175/1520-0485\(1997\)027<0999:sfifn>2.0.co;2](https://doi.org/10.1175/1520-0485(1997)027<0999:sfifn>2.0.co;2)
- Soloviev, A., Lukas, R., & Hacker, P. (2001). An approach to parameterization of the oceanic turbulent boundary layer in the western Pacific warm pool. *Journal of Geophysical Research*, 106(C3), 4421–4435. <https://doi.org/10.1029/2000jc900154>
- Subramanian, A., Ummenhofer, C., Giannini, A., Holland, M., Legg, S., Mahadevan, A., et al. (2016). Translating process understanding to improve climate models (A US CLIVAR White Paper. Report 2016-3, p. 48pp). <https://doi.org/10.5065/D63X851Q>
- Thyng, K. M., Greene, C. A., Hetland, R. D., Zimmerle, H. M., & DiMarco, S. F. (2016). True colors of oceanography: Guidelines for effective and accurate colormap selection. *Oceanography*, 29(3), 9–13. <https://doi.org/10.5670/oceanog.2016.66>
- Umlauf, L., & Burchard, H. (2003). A generic length-scale equation for geophysical turbulence models. *Journal of Marine Research*, 61(2), 235–265. <https://doi.org/10.1357/002224003322005087>
- Umlauf, L., Burchard, H., & Bolding, K. (2005). GOTM—Scientific documentation. Version 3.2 (Technical Report No. 63). Warnemünde, Germany: Leibniz-Institute for Baltic Sea Research.
- U.S. CLIVAR Office. (2008). *Review of U.S. CLIVAR Pilot Climate Process Teams, and Recommendations for Future Climate Process Teams Report 2008-3*, p. 6pp. Washington, DC: 20006, U.S. CLIVAR Office. Retrieved from <https://usclivar.org/sites/default/files/CPTReview-doc.pdf>
- U.S. CLIVAR Scientific Steering Committee (2002). Climate Process Modeling and Science Teams (CPTs): Motivation and Concept (Report 2002-1, p. 4pp). Washington, DC: 20006, U.S. CLIVAR Project Office.
- Wang, D., Large, W. G., & McWilliams, J. C. (1996). Large-eddy simulation of the equatorial ocean boundary layer: Diurnal cycling, eddy viscosity, and horizontal rotation. *Journal of Geophysical Research: Oceans*, 101(C2), 3649–3662. <https://doi.org/10.1029/95JC03441>
- Wang, W., Kumar, A., Fu, X., & Hung, M.-P. (2015). How important is the sea surface temperature uncertainty in the prediction of tropical convection associated with the MJO? *Monthly Weather Review*, 143, 3156–3175. <https://doi.org/10.1175/MWR-D-14-00385.1>
- Warner, S. J., & Moum, J. N. (2019). Feedback of mixing to ENSO phase change. *Geophysical Research Letters*, 43(13), 927–13927. <https://doi.org/10.1029/2019GL085415>
- Weaver, S., Wang, W., Chen, M., & Kumar, A. (2011). Representation of MJO variability in the NCEP climate forecast system. *Journal of Climate*, 24, 4676–4694. <https://doi.org/10.1175/2011jcli4188.1>
- Woolnough, S. J., Slingo, J. M., & Hoskins, B. J. (2001). The organization of tropical convection by intraseasonal sea surface temperature anomalies. *Quarterly Journal of the Royal Meteorological Society*, 127, 887–907. <https://doi.org/10.1002/qj.49712757310>
- Yokoi, S., Katsumata, M., & Yoneyama, K. (2014). Variability in surface meteorology and air-sea fluxes due to cumulus convective systems observed during CINDY/DYNAMO. *Journal of Geophysical Research: Atmospheres*, 119, 2064–2078. <https://doi.org/10.1002/2013JD020621>
- Yoneyama, K., & Zhang, C. (2020). Years of the Maritime Continent. *Geophysical Research Letters*, 47, e2020GL087182. <https://doi.org/10.1029/2020GL087182>

- Yoneyama, K., Zhang, C., & Long, C. N. (2013). Tracking pulses of the Madden–Julian oscillation. *Bulletin of the American Meteorological Society*, 94, 1871–1891. <https://doi.org/10.1175/BAMS-D-12-00157.1>
- Zaron, E. D., & Moum, J. (2009). A new look at Richardson number mixing schemes for equatorial ocean modeling. *Journal of Physical Oceanography*, 39, 2652–2664. <https://doi.org/10.1175/2009jpo4133.1>
- Zeng, X., Zhao, M., & Dickinson, R. E. (1998). Intercomparison of bulk aerodynamic algorithms for the computation of sea surface fluxes using TOGA COARE and TAO data. *Journal of Climate*, 11(10), 2628–2644. [https://doi.org/10.1175/1520-0442\(1998\)011<2628:IOBA>2.0.CO;2](https://doi.org/10.1175/1520-0442(1998)011<2628:IOBA>2.0.CO;2)
- Zhang, C., Dong, M., Hendon, H. H., Maloney, E. D., Marshall, A., Sperber, K. R., et al. (2006). Simulations of the Madden–Julian oscillation in four pairs of coupled and uncoupled global models. *Climate Dynamics*, 27(6), 573–592. <https://doi.org/10.1007/s00382-006-0148-2>
- Zhang, C., Gottschalck, J., Maloney, E. D., Moncrieff, M. W., Vitart, F., Waliser, D. E., et al. (2013). Cracking the MJO Nut. *Geophysical Research Letters*, 40, 1223–1230. <https://doi.org/10.1002/grl.50244>
- Zhang, C., & Anderson, S. P. (2003). Sensitivity of intraseasonal perturbations in SST to the structure of the MJO. *Journal of Atmospheric Sciences*, 60, 2196–2207. [https://doi.org/10.1175/1520-0469\(2003\)060<2196:soipis>2.0.co;2](https://doi.org/10.1175/1520-0469(2003)060<2196:soipis>2.0.co;2)
- Zipser, E. J. (1977). Mesoscale and convective-scale downdrafts as distinct components of squall line structure. *Monthly Weather Review*, 105(12), 1568–1589. [https://doi.org/10.1175/1520-0493\(1977\)105<1568:macdad>2.0.co;2](https://doi.org/10.1175/1520-0493(1977)105<1568:macdad>2.0.co;2)
- Zuidema, P., Torri, G., Muller, C., & Chandra, A. (2017). A survey of precipitation-induced atmospheric cold pools over oceans and their interactions with the larger-scale environment. *Surveys in Geophysics*, 38(6), 1283–1305. <https://doi.org/10.1007/s10712-017-9447-x>